Flexible Touchpads Based on Inductive Sensors Using Conductive Composite Polymer and Flexible Metal PCB

by

Alireza Rahbar

B.Sc., Simon Fraser University, 2012

Thesis Submitted in Partial Fulfillment of the
Requirements for the Degree of
Master of Applied Sciences

in the
School of Engineering Science
Faculty of Applied Sciences

SIMON FRASER UNIVERSITY

Spring 2015

Approval

Name:	**Alireza Rahbar**
Degree:	**Master of Applied Sciences**
Title:	***Flexible Touchpads Based on Inductive Sensors Using Conductive Composite Polymer and Flexible Metal PCB***
Examining Committee:	**Chair:** Michael Sjoerdsma Senior Lecturer, School of Engineering Science

Bonnie L. Gray, P. Eng
Senior Supervisor
Associate Professor _____

Carlo Menon, P. Eng
Supervisor
Associate Professor _____

Andrew Rawicz, P. Eng
Internal Examiner
Professor
School of Engineering Science _____

Date Defended/Approved: March 11, 2015

Partial Copyright Licence

Abstract

In this thesis, the design, fabrication, testing and characterization of two tactile sensor array technologies are presented. The two sensor systems both use inductance as a transduction principle and are designed to be implemented in flexible wearable systems. The tactile sensor arrays feature flexible PCB substrates and/or flexible conductive composite polymer (CCP) structures, resulting in highly flexible tactile arrays. Each switch consists of 4 elements: fascia, target, spacer and a sensor coil. The user presses the fascia, bringing the target in contact with the sensor coil. In the first method, where the system operates based on the principle of eddy current generation, movement of the conductive target changes the inductance of a sensing coil. In the second method, the contact between the target and the conductive membrane triggers a touch detect in the detection mechanism. An electronic circuit that accurately measures inductances is developed to detect the change in the inductance of each sensor's coil when the user presses the target element of the sensor. Different sizes and geometries of coils in both flexible PCB metal and CCP are investigated to determine which couple best with the CCP that forms the target for the inductive coils. Using COMSOL, a COMSOL simulation of the coil geometries is also conducted in order to study the generated magnetic field and distribution of the magnetic flux density at the center of the coils. Techniques for patterning two-layer inductive coils on flexible PCBs are described. A low cost microfabrication technique to create inductive flexible coils using embedded CCP in polydimethylsiloxane as an alternative to PCB metal coils is also presented. The inductance for a sensor composed of PCB metal coils and CCP target are measured to be approximately 33.1 μH and 42.9 μH for circular and square geometries, respectively, before being pressed. When pressed, a 40% change in the inductance is observed, a change which is easily detected. In the case of coils made of CCP, although the measured inductance values are shifted because of the internal resistance of the coils, a 35% change in the inductance was observed when the conductive target was pressed.

Keywords: flexible sensor; touchpad; tactile sensor; flexible coils; conductive polymer; microelectromechanical systems; wearable sensors

Acknowledgements

I would like to offer my sincere gratitude to my supervisor Dr. Bonnie Gray for her incredible support, valuable feedback and guidance. Her patience, expertise, understanding and encouragement made this work possible. Additional thanks to my thesis committee members Dr. C. Menon and Dr. A. Rawicz for their contribution. I would like to further extend m*y* sincere gratitude to Dr. Menon for giving me access to his lab equipment.

A very special thanks goes to my sister and mentor Mona. It was because of her encouragement that I applied for graduate school. Through her continues support, training and untiring guidance I was able to finish this work. Thanks are extended to Paul Stoffregen, Nezam Alavi and Nicholas Doyle for their help thought this project.

I would also like to thank my family for the support they provided me throughout my life. My parents, Fakhri and Ali, my sister Mona and my brother Eric to whom this work is dedicated to, have been a constant source of love and encouragement. Without them, I would not have been able to be where I am today.

Finally I would like thank Canadian Foundation for Innovation (CFI) and CMC Microsystems for funding, equipment, and software, which made this research possible.

Table of Contents

List of Tables

List of Figures

List of Acronyms

CAD	Computer-Aided Design
CCP	Conductive Composite Polymer
CTC	Clear Timer on Compare
DI	Deionized
EMF	Electromotive Force
FEA	Finite Element Analysis
GDSII	Graphic Data System – version II
LIGA	Lithographie Galvanoformung Abformung
MEMS	Microelectromechanical Systems
PDF	Portable Document Format
PVDF	Polyvinylidene fluoride
PWM	Pulse Width Modulation

Chapter 1.

Introduction

A tactile sensor is defined as a device that is capable of measuring the properties of contact between the sensing device and an external stimuli [1]. These properties may include contact, force, the shape of the object, texture, temperature and other physical characteristics [2], [3]. Most important functional categories of tactile sensors are manipulation, exploration and response. The most common measurands are contact and force. By placing individual devices (called *tactels*) into an array, as shown in Figure 1.1, or via movement of a single tactile sensor element, other information can be obtained such as the shape of an object or its texture. The basic concept behind a tactile sensor is shown in Figure 2. Tactile sensors are widely used for tasks that range from simple touch detection, to robotic manipulation of objects requiring complex feedback mechanisms. By direct contact between the sensor and the object, some tactile sensors are capable of sensing properties such as shape, pressure distribution, texture, slippage, thermal properties [3]. Tactile sensing is well-established in a variety of applications across a number of domains that include robotics, biomedicine, and wearable devices, where such contact information is important for object sensing, manipulation, and feedback control.

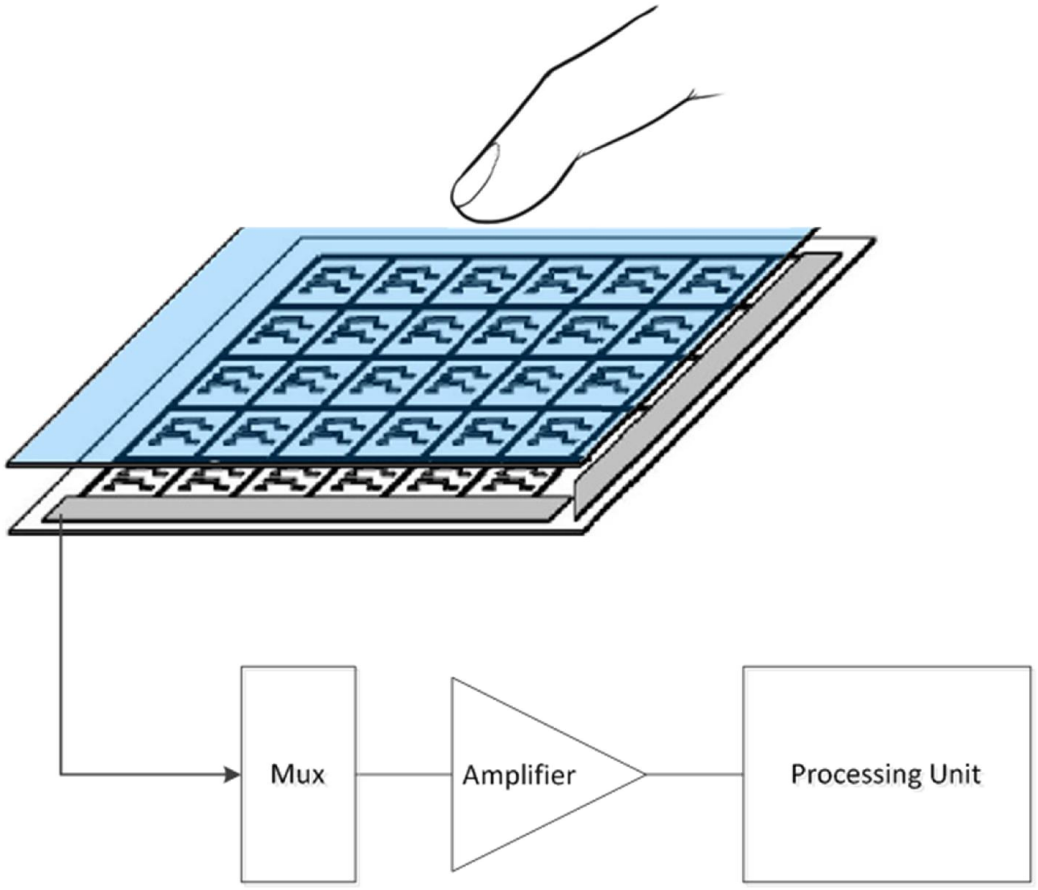

Figure 1.1: An array of tactile sensors. Each individual square is a tactel. The blue interface represents a low pass special filter in the form of rubber.

The performance of a tactile sensor is evaluated based on the following properties: sensitivity, dynamic range, hysteresis, linearity, signal-to-noise ratio, response time, reliability, elasticity, robustness, and spatial resolution. Based on the application requirements, each system is designed to meet some of the standards defined by these properties [4]. A tactile sensor array consists of an array of individual sensors arranged in homogeneous matrices that together form a sensitive site. When the information coming from each individual sensor is combined, the system is capable of conveying information about the state of touch such as texture, slip and other properties. By miniaturizing the sensor elements, the array can be densified to increase the spatial resolution and sensitivity of the tactile sensor array.

A variety of tactile transduction techniques that are based on different principles exist for a wide variety of applications. In Section 1.1.1, these methods are presented, along with a short discussion of applications of tactile sensors in Section 1.1.3. In Section 1.2, shortcomings in these methods are then discussed to provide motivation for the research presented in this thesis in which tactile sensing is achieved by the fabrication and patterning of composite polymers to realize fully-flexible polymer based inductive tactile sensors. These new sensors are designed to not only address some of the shortcomings of previous methods, but are designed within the context of tactile sensors that are compatible with wearable technologies.

1.1. Background

1.1.1. Tactile Sensing Transduction Methods

As mentioned previously, a wide range of tactile transduction techniques that are based on different principles exist with the simplest being a direct contact swtich. Below, some of the most important methods of tactile sensing are described by briefly summarizing the prior work done in the field, and then describing the advantages and disadvantages of each method in terms of various relevant parameters such as performance, flexibility and suitability for wearable systems, ease of fabrication, and complexity of drive and read-out circuitry.

Resistive sensors: Resistive tactile sensors work based on the principle that electric resistance of an elastic conductive material changes under applied pressure. A variety of techniques have been used to implement resistive sensors. For example, conductive polymers, most commonly carbon or silicon doped rubber, have been used as an elastomer to fabricate resistive tactile sensors [1]. The sensing mechanism for these polymer-based sensors involves measuring the resistance across a section of an elastic material. The electric resistance changes under applied force since the cross section of the membrane decreases while its conduction length increase. Due to their simplicity, resistive sensors are very easy to fabricate and can be made to be flexible; however they have disadvantages such as long time constant, poor long term stability, nonlinear force versus resistance behavior and high hysteresis.

Another type of resistive tactile sensor utilizes the piezoresistance property of semiconductors by which the electric resistance of the semiconductor changes with applied strain. The piezoresistance of the semiconductor material is a function of the mobility of the charge carriers which itself changes by the volume of the material. This sensing technology is widely used because of its low fabrication cost and high sensitivity [2], [5]. However because of the nature of this transduction mechanism, the mobility of the charge carriers in the piezoresistive material changes with temperature and therefore temperature compensation mechanisms are required, which adds to the complexity of the sensor and read-out circuitry design [2].

Capacitive sensors: Capacitive sensors consist of two conductive parallel plates that are separated by a dielectric material. The capacitance, *C*, between the plates is inversely proportional to the distance between the two plates. With applied force/pressure, the structure deforms and therefore the distance between the plates alters resulting in a change in capacitance. Capacitive sensors exhibit high sensitivity, good frequency response, high spatial resolution, low temperature sensitivity, and a large dynamic range. Also, some variations of the capacitive sensors can be made of flexible materials. However, they are susceptible to noise and suffer from crosstalk in array formation, therefore requiring complex signal processing and noise reduction [2], [6].

Piezoelectric sensors: Piezoelectric sensors convert an applied force into an electric voltage by developing an electric charge, proportional to the applied pressure, on their surface [2], [7], [8]. Because of this, piezoelectric sensors do not require a power supply and therefore can be used in a variety of applications. In addition, some piezoelectric materials exhibit a high sensitivity to very small deformations. However, this transduction mechanism is only suitable for detecting dynamic forces, as the output voltage of the sensor decays to zero over time [7], [9]. Commonly used piezoelectric materials include polyvinylidene fluoride (PVDF) polymers, zinc oxide(ZnO), and lead zirconate titanate (PbZrTiO3 or PZT) [7], [10], [11]. PVDF piezoelectric materials are commonly used because of their flexibility, light weight, high piezoelectric coefficients, dimensional stability and chemical inertness [7], [10], [11]. However, such sensors suffer from cross talk when in arrays since the applied pressure tends to propagate over to

adjacent sensing element resulting in a limited resolution [2], [12]. Moreover, they have a high probability of being effected by hysteresis [2], [13].

Optoelectric Sensors: Optoelectric sensors consist of a light source, an optically conductive medium, and a photodetector. One method of transduction is to use the photoelasticity property of media such as polyurethanes or acrylic resins where applied stress changes the polarization plane of the passing light. Subsequently, this changes the intensity of the light, detected often by a camera or a photodiode, and can be correlated to the applied force [2]. Optoelectric sensors have high spatial resolution and are immune to external electromagnetic interferences [2], [14]. However, they are usually bulky and lack flexibility due to the optics involved. In addition, construction of a dense array of these sensors becomes very complex as the array grows: for instance, camera-based optical sensors are usually large and require complex algorithms and high processing power [7].

Inductive Sensors: Inductive coil sensors, which are sometimes called search coil sensors, pickup coil sensors, or magnetic antennae, are one of the oldest and well-known types of magnetic sensors. Inductive coil sensors are often used in non-destructive testing, proximity sensors, current sensors, and other applications. Inductive tactile sensors are a more specific application of this type of transduction. Tactile sensors, using inductive transduction, are demonstrated by [15] and [16], where the sensors are driven by a change in the magnetic flux density of a sensor coil, caused by proximity of a permanent magnet. Another method uses a primary coil which induces a magnetic field sensed in a secondary sensing coil [17]. The mutual inductance of the coils varies as a consequence of the applied load and therefore the amplitude and phase of the voltage measured in the sensing coil can be correlated with the applied load or displacement of the diaphragm [15]–[17]. As a result, the performance of the sensor system can be easily calculated due the simplicity of its transfer function $V = f(B)$ where V and B are the voltage and magnetic field measured in the sensing coil, respectively, and do not include potential external influencing factors such as temperature [18]. However, while these results showed that inductive-based sensors have many advantages, these particular sensors were all very bulky and not flexible.

Another type of sensor that uses magnetic inductive as its operation principle is the displacement sensors. Although displacement sensors can be used as tactile sensors, these sensors are primarily used in industry to monitor the position, proximity and movement of an object, and typically fall under the category of proximity sensors. This type of sensor operates based on the principle of eddy currents, where the sensor coil creates a magnetic field that induces eddy currents in the target. Eddy currents are electric fields produced in a conductive material by a time varying magnetic field, that result in circular electric currents [19]. For more details please see Section 2.1. Displacement of the target changes the magnetic field, which in turn changes the inductance of the coil, resulting in in a simple transfer function where the performance of the coil can be precisely calculated. Surface and sub-surface crack detection are other common applications of eddy current sensors, where micro-cracks in a target structure interfere with the generated eddy current, changing the magnetic field. Although these types of inductive sensors are commonly used in the industry, they have an unexploited greater potential in the emerging areas such as wearable devices [20].

1.1.2. Summary of Touch Sensor Operation Principles

As described above, each sensing principle has its own advantages and disadvantages. Among all the sensor types mentioned, capacitive and inductive sensors show the best performance, reliability and ease of fabrication. However, since they are susceptible to noise and crosstalk, capacitive sensors require complex circuitry to perform signal processing to achieve the required performance. This is the reason they have dominated the computer electronics industry where processing power to perform the required signal processing is considered abandoned. However in wearable systems where the size of the system is a huge factor in the success of the product, inductive sensors are the logical choice due to their simplicity. For example an easy to fabricate, inexpensive glove type of wearable device requires conformal sensors, flexibility, compact read-out circuitry and reliable performance that all can be archived by a miniaturized array of inductive sensors.

1.1.3. Example Applications of Tactile Sensors

Tactile sensors have found many applications in fields that range from robotics and industrial automation to medical applications. These application areas benefit from tactile sensors because these sensors are primarily used as analytical tools that provide feedback during a process to the engineers, technicians and doctors, providing input that allows more control. Some of the most important applications of tactile sensors are described below:

Minimally Invasive Surgery (MIS): MIS is performing a medical surgery through small incisions and typically involves use of specially designed instruments and viewing equipment [9]. One significant drawback of MIS is the increased chance of intra-operative injury due to the loss of haptic feedback that in a normal operation helps the surgeon to explore and manipulate the tissue [21], [22]. Tactile sensors allow remote assessment of patient tissue and can give information about properties such as tissue compliance, viscosity and surface texture to the surgeon for a safer and more effective operation [23].

Diagnostic screening: Tactile sensors can be used in palpatory diagnosis (detection of medical problems via touch) to assess the quality of soft tissues. These sensors can measure different tissue qualities and attributes, such as elasticity and stiffness, that can help in diagnosing cancer; this is because cancerous tissue has several different palpation characteristics from healthy tissue.

Prosthetic limbs: Amputees currently using prosthetics lack the sensation of touch in their prosthetic limbs. The use of tactile sensing helps to restore these sensations and allows amputees to grasp objects in a better-controlled manner. This can help the patient to accept the prosthetics better and greatly improve their quality of life.

Automated industries: Tactile sensors can be used in assembly lines, manufacturing facilities, machining tools, and a variety of other industrial applications where they provide feedback to the control system and facilitate system automation.

Robotics: Tactile sensors are widely used in robotics in a wide variety of configurations. Tactile information is primarily used for object manipulation and to improve the dynamics and control of the robotic system to further improve the performance of the robot. With the feedback supplied by tactile sensors, robotic arms are able to identify, grasp and safely manipulate the objects. When grasping an object, the feedback system aided by tactile sensors can conserve energy while optimizing the forces applied, thus keeping the object from being damaged.

Wearable systems: Recent developments in wearable sensor systems have led to a number of applications. Biomedical engineers have developed a tactile sensor for a wearable force plate that can be used for the early diagnosis of plantar fasciitis, as well as for a proactive treatment of the disorder [24]. Kramer et al. demonstrates a pressure sensitive film that can be integrated into textiles through consumer electronics embedded in clothes [25]. Currently, a new wearable fabric tactile sensors is being developed that can expand wearable sensor systems into every human-life activity which can lead to realization of ubiquitous computing [26].

1.2. Motivations of This Work

The main aim of the work presented in this thesis is to develop a polymer based flexible array of sensor switches intended for applications in wearable electronics and sensor systems. The proposed switches are intended to operate based on an inductive transduction mechanism, and feature flexible conductive composite polymer (CCP) structures and/or thin film metal, resulting in highly flexible switch arrays appropriate for wearable systems. By alleviating some of the shortcomings of the existing tactile sensors, we aim to develop an inductive sensor that is simple in design, not bulky, requires simple signal processing, is temperature independent and is repeatable and shows long term stability. To achieve these goals, an inductive sensing approach was chosen to combine all these characteristics into a single sensor system.

Existing inductive sensors have good dynamic range but, as stated previously, are often bulky in size. Systems that use mutual inductance of two coils also have lower repeatability, as coils don't always return to their original position because of their size

[27]. In many inductive sensors, the primary coil is excited with an alternating current, producing an output voltage on the sensing coil with the same frequency. Although they require simpler read-out circuitry compared to capacitive sensors, detecting the slightest change in voltage requires more complex circuitry, since the alternating signal amplitude must be demodulated [27]. In addition, existing inductive sensors are not flexible and therefore cannot be integrated with wearable electronics devices.

In this thesis we demonstrate and compare two ways to achieve a flexible tactile sensor using inductive principles. In the first method, we show a tactile sensor element that works based on the principle of eddy current generation. A conductive membrane, which is part of the sensor's interface, is deflected by the user's pressure on the interface. Deflection of the conductive target changes the measured inductance value of a sensing coil through the generation of eddy currents. The closer the conductive target is to the sensing coil, the greater the influence of the eddy currents on the inductance of the coil. As a result, the displacement of the target can be correlated with the change in the inductance, in order to predict the location of the membrane with respect to the sensing coil. This method can also be used as a proximity sensor, where the sensing mechanism can detect the proximity of any conductive material, not just the sensor's interface.

The second method uses the contact between the conductive target and the sensing coil to detect a touch. This approach results in a binary switch that can detect two states: contact and non-contact. This sensor system consists of a conductive membrane fabricated using conductive composite polymer or a thin layer of conductive metal embedded in the membrane. The sensing coils are fabricated using both flexible printed circuit board (PCB) as well as polymeric coils made from conductive composite polymer (CCP). When the conductive membrane comes into contact with the sensor coil, it shortens the path between the line traces that form the sensing coil, resulting in a change in the geometry of the coil that has an inductance value significantly different from that of the original state of the coil. The sudden change in the inductance value of the sensing coil triggers a touch detect in the detection mechanism.

In both cases, individual tactile elements are designed, fabricated, and tested, as well as fabricated into small arrays, in order to show the possibility of developing wearable arrays of the sensors for a variety of potential wearable systems applications from acting as a simple on/off control switch to pressure sensitive keypad and further integration with soft orthotics smart fabrics and integrated circuits [25].

1.3. Thesis Objectives

This thesis aims to contribute to the existing field of tactile sensing through the following objectives:

1. Development of two tactile sensor array technologies (eddy-current and binary-switch based) that use inductance as a transduction principle that can be implemented in flexible wearable systems.

2. Development of a general fabrication process for inductive tactile sensors using flexible printed circuit board (PCB) technology, as well as micromolding processes of conductive composite polymers on flexible polymer membranes.

3. Development of a modeling framework for design of inductive sensor coils using finite element analysis tools to study the characteristics of their generated magnetic field.

4. Development of a detection system in the form of both software and hardware that interfaces with a flexible inductive sensor array that can detect and respond to user stimulus.

1.4. Thesis Organization

This thesis is divided into five chapters describing background, design, simulation, and fabrication and characterization of inductive based sensor switch array. Chapter 1 (this chapter) covers introduction and background. Chapter 2 covers the sensor operating principle and general design of the sensor system. Furthermore, it discusses the use of different sizes and coil geometries (square, circular, hexagonal and octagonal) to determine which couple best with the CCP that forms the target for the inductive coils. Other design parameters that would influence the operation of the sensor

such as quality factor and flux density are investigated. Also in Chapter 2, the computer simulation results for the inductive coils, employing circular and square geometries based on the design parameters, are presented. The simulation results validate the recommendations and assist in the development of a final system design. This chapter also discusses the detection circuitry and describes methods used to multiplex the design in order to achieve a bigger array of sensors without adding extra detection circuitry. Furthermore, custom algorithms that are used in the microcontroller are described that perform frequency measurements and report if a touch has been triggered based on the pre-defined conditions.

Chapter 3 gives an in-depth explanation of the development of a technology for patterning two-layer miniaturized inductive planar coils on a flexible PCB. As an alternative to flexible PCB coils, a soft lithography based fabrication technique employing highly flexible CCP is described that creates inductive coils on a flexible PDMS substrate that are both elastic and usable in systems requiring conformal sensors. Finally, the fabrication process for creating the interface segment of the system by using conductive composite polymer or by embedding thin copper layer in the membrane is detailed.

Chapter 4 presents the testing results showing operation of the sensors in the 2 by 2 array. It also covers characterization of electrical properties of the conductive composite polymer. Resistivity of test structure and change in the inductance of the coils were tested during flexing the structures to simulate conditions similar to when the sensor system might be used in a real life application.

Finally, Chapter 5 gives an insight into the future work and presents the contribution of this research.

Chapter 2.

Design of Individual Sensors

This chapter describes the design concept of both sensor system designs: the design that operates based on the generation of eddy currents, as well as the touch sensor design that measures the change in the inductance via change in the geometry of the sensor. In each section, aspects of the design that are the same or different for each sensor type will be discussed in detail. Following an overview of the transduction principle for each sensor type, an analysis of the resonant frequency of the oscillator (which is the centerpiece of the sensor system and detects the physical stimuli) is presented. Sensor coil design considerations are discussed and a Finite Element Analysis (FEA) of the sensor coils is presented in order to help with the understanding of the sensor elements and what design parameters affect them, in order to optimize future designs.

Henceforth, the two different sensor designs will be called the *eddy current sensor* and the *binary switch sensor*, respectively. The designs of the eddy current sensor and the binary switch sensor are very similar. Each tactile sensor (tactel in each array) consists of 4 elements: fascia, target, spacer and a sensor coil. The three elements of fascia, target and spacer together form the interface with which the user interacts. These elements are all fabricated in a flexible polymeric material. The electromagnetic coil for each sensor is formed in a flat spiral shape and, once connected to an electric current, generates a magnetic field and acts as an inductor. Implementation of the coil is done by patterning the coil structure in the copper traces of a flexible PCB, or on flexible polydimethylsiloxane (PDMS) using molding of conductive composite polymer (CCP). The interface is also fabricated by embedding a thin layer of conductive metal (such as aluminum or copper) in the elastomer (PDMS), or by casting

a layer of CCP in PDMS. An example sensor design in shown in Figure 2.1, where the sensor coils are made from flexible CCP.

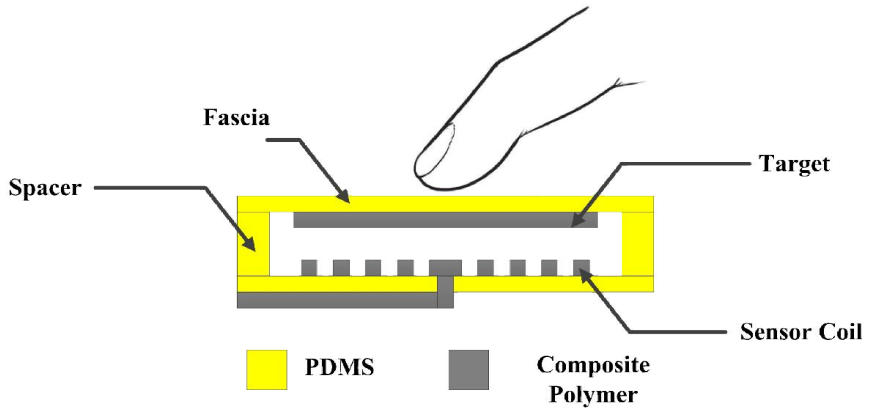

Figure 2.1: Cross sectional view of a single inductive touch sensor employing CCP for the coil. Other designs employ flexible PCB for the coil [28]. Design not shown to scale.

As shown in Figure 2.1, the top layer of the sensor is the fascia and is made from flexible PDMS. It is the surface that the user presses on and may include labels to, e.g. show a control key's functionality. Since it also faces the user, it may also be referred to as the *front panel* throughout this document.

The target is located right underneath the fascia and is made of flexible electrically conductive material. During the fabrication of the interface, the target and fascia are physically bonded together and therefore move together. The target, along with the fascia, can deform together and shift axially relative to the coil when the front panel is pressed by the user.

In order to provide separation between the target and the sensor coil, a spacer layer is molded in the design in the form of a rigid support that holds the target just above the sensor coil. These supports allow the user to press and bring the target into proximity or contact with the sensor coil, and help the fascia and the target bounce back to their original position when not pressed via the spring restoring force of the membrane. The spacer is also made of PDMS and is fabricated at the same time, using the same mold, as the previous two elements.

The operation of the sensor system that is based on the eddy current sensors involves changes in the inductance of the sensor coil. When in proximity of a conductive target, the electromagnetic field of the sensor coil expands towards the conductive target and generates eddy currents in the target by interacting with its electrons [29]. The eddy current generates a secondary magnetic field that opposes the one generated by the coil. Since the inductance of the coil is directly proportional to its magnetic field, this results in a reduction in the measured inductance. The system can be modeled by an equivalent circuit as shown in Figure 2.2, where L0 and R0 represent the sensor coil, L1 represents the second magnetic field, and the load Z represents complex resistive losses in the conductive target that are caused by joule heating [30].

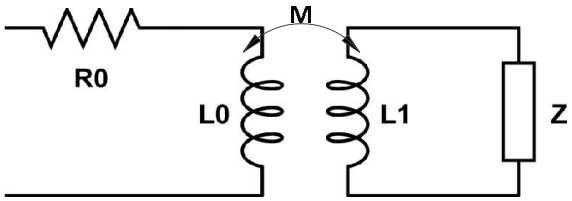

Figure 2.2: Equivalent electric circuit model of the sensor coil with eddy current and resistive losses in the target [28], [30].

When the user touches the fascia and moves the target closer to the coil, the target senses a stronger magnetic field which in turn makes the generated eddy current stronger. A stronger eddy current means a reduction in effective magnetic field of the coil, and therefore a decrease in the inductance of L1.

Without changing many aspects of the design, the eddy current sensor can be transformed into a binary switch sensor that can detect a touch that senses the change in the inductance of the system and is made of flexible polymeric material. Implementation of the coil for this second sensor design is done by casting conductive composite polymer on a PDMS membrane. The interface is also fabricated using PDMS and conductive composite polymer. Table 1 Summarizes different materials used for different sensor designs implemented.

Table 1: Different materials used for different sensors designs implemented.

	Eddy Current sensor	Binary Switch Sensor
Coils system	Flexible PCB	CCP embedded in PDMS or flexible PCB
Target material	Cu or Al Embedded in PDMS	CCP embedded in PDMS

PDMS is a well-researched silicon-based elastomeric thermosetting polymer, widely used in microfluidics and microelectromechanical systems (MEMS). PDMS was chosen for this project because of its many favorable characteristics including: low cost, ease of fabrication via micromolding and soft lithography, ease of sealing between different structures, and mechanical compliancy [31].

FL45 is a two-part silver based conductive composite polymer that consists of a base silver composite and a curing agent (purchased from Zoflex®,USA) that was used as the conductive composite polymer (CCP) material. With a volume resistivity of 0.2 Ω.cm and shore A hardness of 45 (according to company data sheets), FL45 is highly conductive and is quite soft, and results in a flexible structure once cured. Similar to PDMS, FL45 can be micromolded using soft lithography and makes a strong bond to PMDS. One disadvantage of this material, as discussed later in chapter 4, is that it has a higher resistivity compared to commonly used conductors like copper. Because of the internal resistivity of the CCP, formation and movement of eddy currents are limited. Therefore, sensor systems using this CCP does not rely on eddy currents and can only be used as binary switches.

Similar to the eddy current sensor, the flat spiral coil in the binary switch design acts as an inductor. The user presses the frontal panel of the touch switch and brings the conductive target in contact with the sensor coil. Upon contact between the conductive target and the coil, the target shortens the path between the trace lines of the coil and forms a new geometry that has a significantly different inductance, resulting in a measurable change in the inductance of the coil. The changes in the inductance of the coil consequently changes the resonant frequency of the isolator and in turn will be detected by the frequency counter in the detection mechanism.

Both types of sensors have advantages and disadvantages. The binary switch sensor can only detect two states of contact and non-contact but since it is polymer based, it can be easily combined with other polymeric systems, especially those that employ other functional magnetic and conductive composite polymer devices [31]–[34]. The eddy current sensor system can be used as a proximity sensor and has a sensitive region in which a target can be detected. However, because it is fabricated using flexible PCB, it is not stretchable. In addition, although flexible, the PCB is not as flexible as the binary switch's polymers and is also prone to cracks, wear and tear over long periods of use. In choosing which type of switch to use, the particular application in wearable systems would need to be considered.

2.1. Theoretical Design

2.1.1. Eddy Currents and Their Use in the Eddy Current Sensor System

Generation of eddy currents is based on principles of electromagnetic induction. According to the Maxwell-Ampere law, when an alternating current passes through a wire loop, it generates a time varying magnetic field. When the coil excited with an alternating current is placed in proximity of a conductive material, the time varying magnetic field interacts with the electrons of the target in the form of electromotive forces (EMFs) and induces a voltage. As a result of this induced voltage, the electrons experience a Lorentz force that is perpendicular to their motion and therefore veer to the left or right depending on the direction of the field. At the same time, the resistance of the conductor dampens the magnitude of the eddy current and straightens their path [35]. These circular currents created inside the body of the conductor are called *eddy currents*.

The direction of the eddy currents is dictated by Lenz's law. Since we have a varying magnetic field, because of the induced voltage (emf), there will be an induced current whose magnetic field opposes the change in the magnetic flux. For example, if the magnetic field by the coil is decreasing in strength, the induced secondary field will be in the same direction as the first field in order to oppose the change. On the other

hand, if the applied magnetic field is getting stronger, the secondary magnetic field generated will be in the reverse direction to oppose the change in the applied field. Thus, as previously shown in Figure 2.2, we can say that the generated eddy currents and the sensor coil are analogous to two mutually coupled inductors in which the eddy current is model by a secondary coil (L1) whose current direction is opposite of the current in the original sensor coil (L0) [36], [37].

Generation of eddy currents can be exploited for a variety of applications and sensors such as detection of near-surface micro-cracks in metals that disturbs or changes the amplitude or pattern of the eddy current and their resulting magnetic field [38]. On the other hand, the generation of eddy currents can also have undesirable consequences, for example, loss of power due to Joule's law and heat generation. The Joule heating (i.e. Ohmic heating) is undesirable in most applications because it reduces efficiency, creates noise and causes heating of conductive components in the system.

2.1.2. LC Oscillator Model

In this section, we examine the LC oscillator for the eddy current sensor and the alternating current that passes through to create the alternating magnetic field. Figure 2.3 shows a simple LC oscillator circuit where the inductor and the capacitor are in parallel. In this model, it is assumed that the components are ideal and do not have internal resistance.

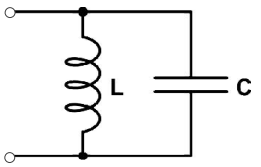

Figure 2.3: Parallel LC circuit. Inductor L represents the sensor coil and C is a known high precision, low-tolerance capacitor.

The voltage across the inductor is defined as V_L and the voltage across the capacitor as V_C. Therefore V_L and V_C are given by:

$$V_L(t) = L\frac{di}{dt}. \quad \text{Equation 1}$$

$$V_C = \frac{q}{C}. \quad \text{Equation 2}$$

where *L* is the inductance of the coil and *C* is the capacitance value of a known high precision, low-tolerance capacitor. By Kirchhoff's circuit laws $V_{L=}$ V_C. Therefore:

$$L\frac{di}{dt} = \frac{q}{C}, \quad \text{Equation 3}$$

Taking the derivative of both sides with respect to time we get:

$$L\frac{d^2i}{dt^2} = \frac{1}{C}\frac{dq}{dt}, \quad \text{Equation 4}$$

$$\frac{d^2i}{dt^2} = \frac{1}{LC}\frac{dq}{dt}, \quad \text{Equation 5}$$

Since $= -\frac{\mathrm{dq}}{\mathrm{dt}}$, this results in:

$$\frac{d^2i}{dt^2} = -\frac{1}{LC}i, \quad \text{Equation 6}$$

Equation 6 is a differential equation which has the following solution:

$$i = I_a \sin(\omega_0 t), \quad \text{Equation 7}$$

where

$$\omega_0 = \frac{1}{\sqrt{LC}}, \quad \text{Equation 8}$$

which represents the resonant frequency of the LC oscillator. The resonant frequency, *f*, can be expressed in Hz by:

$$f = \frac{1}{2\pi\sqrt{LC}}, \qquad \text{Equation 9}$$

Using Equation 1, the voltage across the inductor can thus be calculated:

$$\frac{di}{dt} = \omega_0 I_a \sin(\omega_0 t)\,, \qquad \text{Equation 10}$$

$$V_L(t) = \omega_0 I_a L \sin(\omega_0 t). \qquad \text{Equation 11}$$

2.1.3. Resonant Frequency of a Non-Ideal LC Circuit

Equation 8 gives the resonant frequency for an ideal LC oscillator. As discussed in detail in chapter 4, the fabricated coils using CCP have an internal resistance and, depending on the size of the coil, this internal resistance can change the oscillation frequency of the circuit. Figure 2.4 shows the model that accounts for the internal resistance of the coil and is used to calculate the resonant frequency of the system when CCP coils are involved.

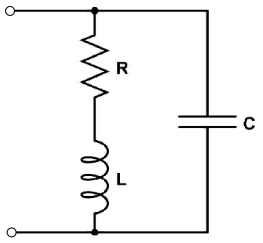

Figure 2.4: *RLC* circuit with parallel capacitor. The internal resistance of the inductor is modeled with a series resistor.

The input impedance of this circuit Z_{in} is given by [39]:

$$Z_{in} = \frac{\frac{1}{j\omega C}(R + j\omega L)}{\frac{1}{j\omega C} + R + j\omega L} \qquad \text{Equation 12}$$

$$= \frac{(R + j\omega L)}{1 - \omega^2 LCP + j\omega CR}\left[\frac{(1 - \omega^2 LCP) - j\omega CR}{(1 - \omega^2 LCP) - j\omega CR}\right]$$

$$= \frac{R}{(1 - \omega^2 LCP)^2 + \omega^2 C^2 R^2} + j\frac{\omega L - \omega^3 L^2 C - \omega CR^2}{(1 - \omega^2 LCP)^2 - \omega^2 C^2 R^2}$$

Setting the imaginary part to zero and solving for the frequency we get:

$$\frac{\omega L - \omega^3 L^2 C - \omega CR^2}{(1 - \omega^2 LCP)^2 - \omega^2 C^2 R^2} = 0 \xrightarrow{yields} \omega = \sqrt{\frac{1}{LC} - \left(\frac{R}{L}\right)^2} \qquad \text{Equation 13}$$

As shown above, in the case of a resistor in series with the inductor, the resonant frequency is not the same as of a simple LC circuit shown by Equation 8. However, when:

$$\frac{1}{LC} \gg \left(\frac{R}{L}\right)^2 \qquad \text{Equation 14}$$

is satisfied the resonant frequency can be approximated to be the same as Equation 8.

2.1.4. Quality Factor and Coil Design

As shown in the previous sections, the polymeric coils are non-ideal and have internal resistance which causes a loss of energy and loss of inductive quality. In addition, the generation of eddy currents in the conductive target material also contributes to energy loss by converting electrical current into heat. In this section, we combine the electric losses in the coil and the target and define the quality factor *Q* for the sensor system as a whole. The quality factor is important as it facilitates optimization of the design such that the energy losses in the system are minimized.

The quality factor, *Q*, describes how underdamped an oscillator is and is defined by [40]:

$$Q = \frac{\omega L}{R}, \qquad \text{Equation 15}$$

where *ω* is the radian resonant frequency, *R* is the inductor's effective series resistance, and *ωL* is defined as the inductive reactance. A higher *Q* indicates a lower rate of energy loss in the LC oscillator circuit and an inductor behavior that is closer to the ideal.

The quality factor can be increased by raising the inductance *L* when increasing the number of turns *N* in the coil (since $L \propto N^2$) and keeping the trace line dimensions the same. On the other hand, more turns means more resistance, but since volumetric resistance is linearly proportional to N with a proportionality factor much smaller than *L*'s, the overall quality factor increases. Therefore, air coils with high quality factor tend to have a large outer diameter and many turns [41].

To examine and reflect the effects of the eddy current, the equivalent circuit of sensor coil and the target is discussed next. Applying Kirchhoff's voltage law to the circuit, as shown in Figure 2.2, we obtain:

$$I_1 R_1 + I_1 j\omega L_1 - I_2 j\omega M = V_L \qquad \text{Equation 16}$$

$$-I_1 j\omega M + I_2 R_2 - I_2 j\omega L_2 = 0 \qquad \text{Equation 17}$$

Hence, the equivalent resistance and inductance is given by:

$$R = R_1 + \frac{\omega^2 M^2}{R_2^2 + (\omega L_2)^2} R_2 \qquad \text{Equation 18}$$

$$L = L_1 - \frac{\omega^2 M^2}{R_2^2 + (\omega L_2)^2} L_2 \qquad \text{Equation 19}$$

The quality factor can thus be obtained by:

$$Q = \frac{\omega L}{R} = \omega \frac{L_1 - \frac{\omega^2 M^2}{R_2^2 + (\omega L_2)^2} L_2}{R_1 + \frac{\omega^2 M^2}{R_2^2 + (\omega L_2)^2} R_2} \qquad \text{Equation 20}$$

$$= \omega \frac{L_1 R_2^2 + \omega^2 L_2 (L_1 L_2 - M^2)}{L_1 R_2^2 + \omega^2 (R_1 L_2^2 - M^2 R_2)}$$

Since $M = k\sqrt{L_1 L_2}$ and *k*≤*1*, then$L_1 L_2 - M^2 \geq 0$ [37].

As a result, increasing *ω* by changing the design parameters in the oscillator (particularly by manipulating the capacitor value, since the above expression is independent of *C*), should improve the quality factor. This is desirable to some extent, as a better quality factor means a lower eddy current generation and less power consumption. However, there is trade off: displacement of the target diaphragm also generates eddy currents. Therefore, when designing the system, the initial magnetic field, when the target is at rest, must be large enough to reach the conductive target. Otherwise, if the magnetic field is weak, it can only cover a portion of the distance between the coil and the target, and will leave a zone where displacement of the target diaphragm cannot be detected since there's no eddy current generated and the inductance remains the same. It is only after the target enters the coil's magnetic field that the system can distinguish displacement of the target.

2.1.5. Design of Inductive Coils

Use of a ferromagnetic core in an electromagnetic coil can make the generated magnetic field significantly larger. The ferromagnetic core, such as one made of iron, is magnetized by the magnetic field of the coil, causing the magnetic domains to line up with each other and generate a field that adds to the coil's field , thus increasing the overall magnetic field by a large factor in the order of hundreds or thousands [42]. However, a coil without a ferromagnetic core has empty air space between the windings, and is called an air coil. Because of their lower magnetic field, air core coils have a relatively lower sensitivity to presence of a target compared to ferromagnetic core coils;

for this application, flat planar air core coils were chosen. This was done primarily because the addition of a ferromagnetic coil complicates the design without significantly improving the functionality of the sensor, whereas flat air coils can be easily fabricated using standard lithography and molding procedures compatible with flexible systems. In addition, using a ferromagnetic core material introduces nonlinearity into the coil's response during temperature and flux density change, which can result in false positives and missed hits [18].

Different geometries, including circular, square, hexagonal and octagonal coils were considered for the design of the air coils (Figure 2.5). The inductance of a planar spiral coil is given by Wheeler's approximation:

$$L = \frac{r^2 n^2}{8r + 11w}, \qquad \text{Equation 21}$$

where *r* is the outer radius of the coil, *n* is number of the turns and *w* is the width of the windings [43]. More accurately, Mohan *et al.* gives an expression to calculate coil inductance for different geometries based on a current sheet approximation:

$$L = \frac{C_1 \mu_0 n^2 d_{avg}}{2}\left[ln\left(\frac{C_2}{\rho}\right) + C_3\rho + C_4\rho^2\right], \qquad \text{Equation 22}$$

where μ_0=4π×10^{-7} (H.m-1) is the permeability of vacuum, *n* is number of the turns, $d_{avg} = \frac{\text{din+dout}}{2}$, $\rho = \frac{\text{dout−din}}{\text{din+dout}}$ is the fill ratio, and the *C* coefficients are given in the table below [44]. Figure 2.5 shows the different coil geometries and how their associated parameters are defined.

Table 2: Coefficients for current sheet approximation [44].

	C1	C2	C3	C4
Circle	1.00	2.46	0.00	0.20
Square	1.27	2.07	0.18	0.13
Hexagonal	1.09	2.23	0.00	0.17
Octagonal	1.07	2.29	0.00	0.19

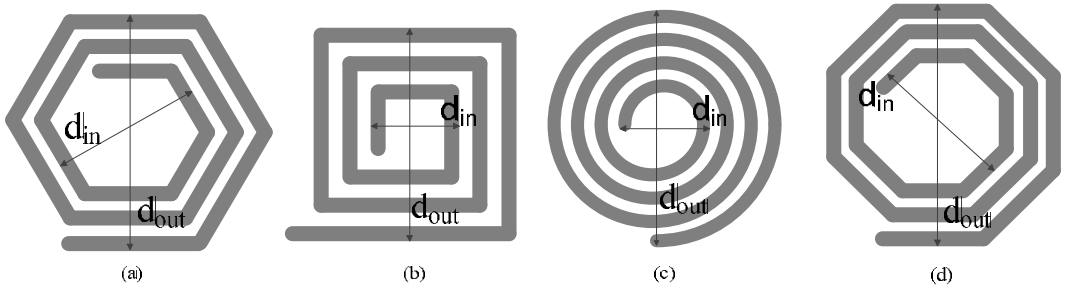

Figure 2.5: Inductor design using (a) hexagonal spiral, (b) square spiral, (c) circular spiral and (d) octagonal spiral. Parameters d_{in} and d_{out} are defined as depicted in the figure [28].

Since the change in inductance is measured through the change in the resonant frequency, to allow for the maximum potential range for the resonant frequency swing, the most desirable geometry is the one that maximizes the inductance. The inductance for each geometry was examined in order to find out which one would give the maximum inductance when fixing other parameters such as number of turns, trace line thickness, etc. As shown by Equation 22 and Table 2, for all the same factors involved, the square geometry is expected to result in the maximum inductance. For example, using Equation 22 for an arbitrary coil with *n*=10 turns and *din*=1 cm and *dout*= 5 cm, the inductance values are calculated to be 3.1379 μH for the square flat spiral coil, 2.6286 μH for the circular flat spiral coil, 2.6361 μH for the hexagonal flat spiral coil, and 2.6592 μH for the octagonal flat spiral coil. As a result, square geometries are the best design choice when designing the sensor coils, since they have the highest inductance for the area they occupy. Therefore, the coils were made using square geometry; for comparison, circular coils were also fabricated.

The design of the inductive coils is limited by the fabrication technology used to create the coils. For the PCB coils fabricated to create the eddy current sensor, the design is limited by the maximum resolution that can be achieved during the fabrication process which with the available equipment is approximately 50 to 100 μm. These limitations determine factors such as line width, and therefore the density of the coil. In the case of binary switch tactile sensors, since the coils are fabricated by casting a conductive polymer in a PMMA mold, they require demolding. The nature of the conductive composite polymer and challenging demolding process limits the maximum

resolution attainable, and as a result of these limitations, the number of turns achievable per unit area also becomes limited. Therefore, the fabricated sensor coils used in binary switches have 7 turns which is lower compared to the ones fabricated using flexible PCB. These limitations were also considered in the final designs of the coils.

2.2. Layout of Sensor Array

A 2×2 array of four sensors was implemented to demonstrate their proof of the concept as both individual and arrayable inductive touch sensors. A two-dimensional sensor array can be easily expanded with no changes in the fabrication process of the sensors. In the case of the eddy current sensor, the coils on the same row or column were placed apart from each other to form a 2x2 array at a distance equal to their outer diameter. Although a closer arrangement of the coils is possible to form a denser array and potentially take advantage of spatial interpolation between elements, this separation was chosen to ensure that there was minimal electromagnetic interference between the coils. Testing the prototypes showed that the distance between two adjacent sensor coils should not be less than the outer radius of the circular coils, or half the side length of the square coils. Figure 2.6 shows the layout design of the eddy current sensor coils employed for fabrication and testing.

The layout of the sensor array for binary switches can be made to be much denser compared to eddy current sensors. The binary switches detect the change in the inductance of the coil caused by the contact between the conductive target and the sensor coil and work independently of the eddy current generation. Therefore, the sensors in the array do not interfere with each other, which allows for bringing the sensor coils closer to one another and thus creating a denser sensor array.

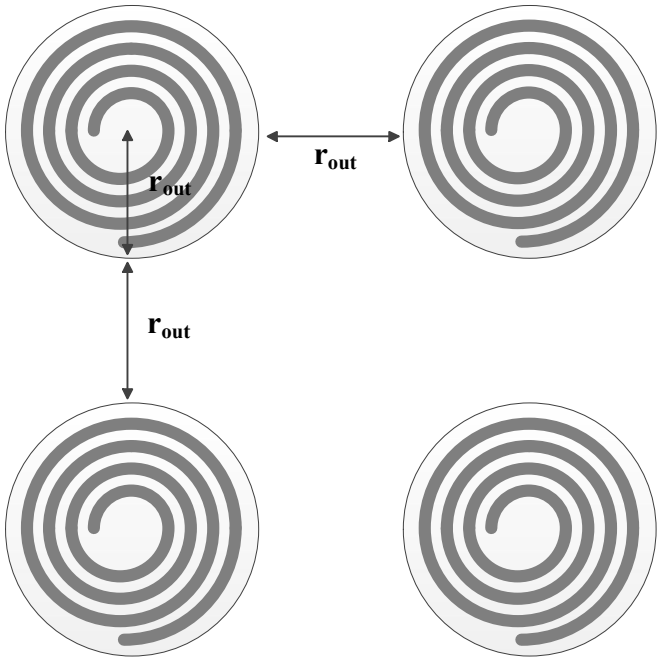

Figure 2.6: Layout of the fabricated 2×2 sensor coil array. The coils are placed with a distance equal to their outer diameter to prevent any possible interference.

2.3. COMSOL Simulation of the Coils

In this section, a simulation model for micro-scale planer circular and square inductors is presented which facilitates better understanding, prediction, and design of the behavior of the sensor system. The purpose of this section is to examine the strength of the generated magnetic field and distribution of the magnetic flux density at the center of the coils. For this simulation, COMSOL, a finite element analysis (FEA) solver and simulation software package for various physics and engineering applications, was employed.

To perform the simulation, a 3D model of the both types of coil structures (circular and square) were created using SolidWorks®, a modeling CAD software produced by Dassault Systèmes SolidWorks Corp. based in Vélizy, France. These geometries were created by first drawing them in two dimensions, and then extruding them to achieve a 3D geometry. Each coil was placed in a bounding box in the shape of a cube to define the boundaries and domains used in COMSOL to model the spiral-

shaped inductor and the air surrounding it. The dimensions for the air subdomain (i.e. the bounding box) can be selected arbitrarily depending upon the size of the structures, but must be kept large enough to allow a reasonable expansion of the magnetic flux further away from the coils. Figure 2.7 shows the modeled inductor coil and the surrounding air subdomain with the inlet and outlet connected to the sides of the bounding box. The bounding box has a dimension of 7mm×7mm×7mm.

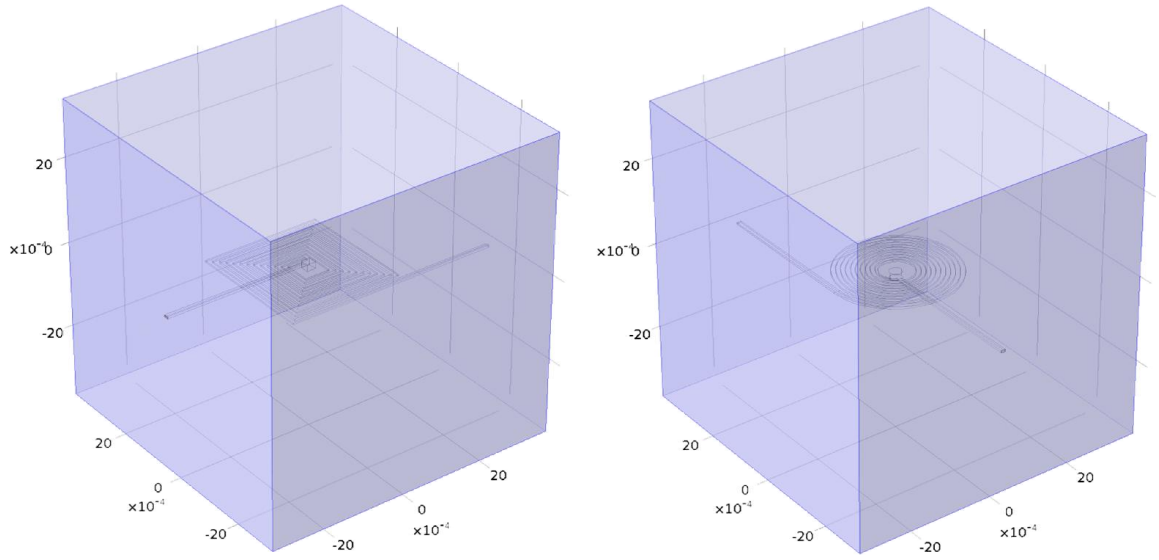

Figure 2.7: The modeled square and circular coil geometries with their surrounding air subdomain. The inlet and outlet connections of the coil are in contact with the bounding box. The bounding box cube has a side length of 7mm.

The simulated coils are similar to those fabricated by CCP and on PCB in terms of shape and line to spacing ratio, but are slightly scaled down to also give a representation of the behavior of the generated magnetic field for the future miniaturization of the coils. Both circular and square coil geometries had 6 turns and formed a 3 mm by 3 mm square or circular 3-mm-diameter micro-coil with a one-to-one line to spacing ratio. The line thickness of the modelled conductor was 40 μm with a line width of 100 μm.

COMSOL's AC/DC Module, a dedicated tool package for simulating electric, magnetic, and electromagnetic fields in static and low-frequency applications, was used to simulate the inductor coils [45]. The system was modeled in two steps, where in the

first step the current density vector in the inductor was calculated. In the second step, the magnetic flux was calculated by using the current in the first step as the source. A passing current of 10 mA was sent through the inlet of the coil. This current was chosen because of its being a reasonable amount that could be applied by on-chip wearable microelectronics and/or field-programmable gate array (FPGA) [31]. In all cases, mesh-independence of results was assured.

There were three boundary conditions for this model: (1) Input inlet (connected to the current as previously described), which is magnetically insulating boundary with a port boundary condition. (2) Output outlet, which again is a magnetically insulating boundary, but also has a constant potential of 0V. (3) The air surrounding the coil, which is both magnetically and electrically insulating.

The electric conductivity of the material was set to be 5.85×10^{7} S/m, which is the conductivity of copper. The conductivity of air is arbitrary, but must be set to a small value to avoid singularities in the solution. The conductivity of air was set to be 1 S/m for this simulation (compared to its actual value of 2×10^{-14}, which is much smaller than the conductivity of the copper and so results in a negligible error in the calculations, yet doesn't cause singularities).

Error! Reference source not found. shows the simulated magnetic flux density in the air surrounding the square and circular 3 mm by 3 mm coil. The field lines are depicted by the streamline, and because it is a vector field quantity, it is strongest near the center of the coil; this is because it is the vector sum of all the field lines nearby, resulting in a higher flux density at the center. The magnetic flux density at the center of the coil was computed to be approximately 82.4 μT and 99.7 μT for the circular and square inductor coil geometry, respectively, with an input current of 10 mA.

The previously described boundary condition imposed on the bounding box of the model causes the field lines to bend away from their original path and follow the contours of the box. This consequently resulted in an error in the calculated filed lines and inductance of the coil. Although the error is negligibly small because of the smallness of the field near the surface of the bounding box, it proved possible to minimize the error by enlarging the bounding box. Also shown in **Error! Reference**

source not found. is the simulated electric potential distribution on the surface of the inductors by using thermal coloring style, where the light yellow indicates a higher voltage potential at the input inlet (approximately 200 mV for both coils) and dark red indicates a voltage potential close to zero near the output outlet of the coil geometry.

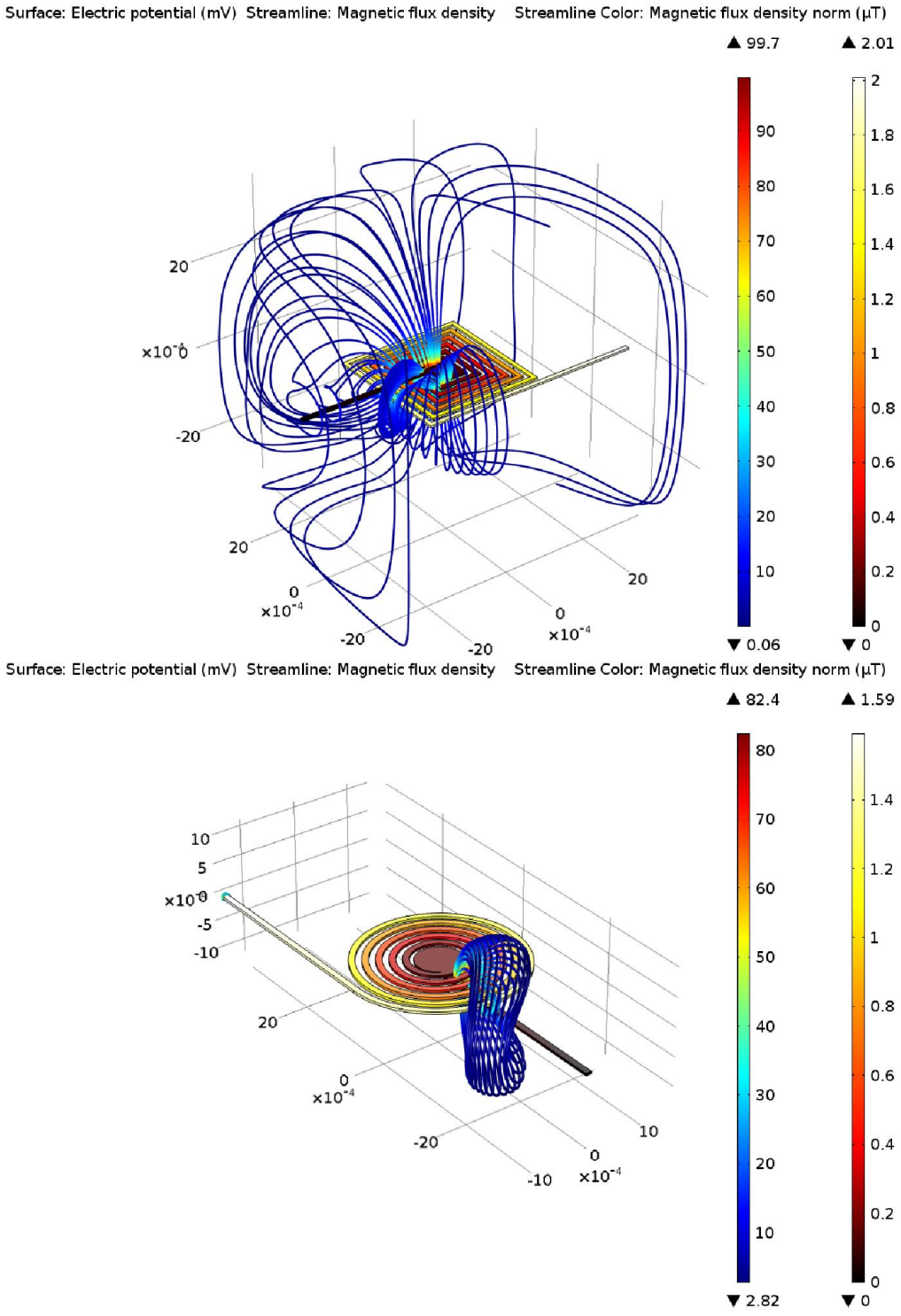

Figure 2.8: **COMSOL simulation of the square (top) and circular (bottom) flat micro coils. Colors on the surface of the coil represent the electric potential (V). Streamlines shows the distribution of the magnetic field line and their flux density norm (μT).**

As previously mentioned, the magnetic flux density drops rapidly when moving away from the coil's surface. This is desirable in the system since a lower flux density means that a lower eddy current is generated in the conductive target, which in turns means that there is lower power consumption when in an idle position. For applications where the distance between the target and the coil is greater and therefore a higher flux density is required, the input current can be raised to increase the flux density of the coil. As previously stated, the flux density is greatest near the surface of the coil and thus so is the magnetic field generated by the field. As a result, we expect the sensor's response to be the most sensitive near the surface of the coil where the magnetic field is the greatest. This will be further examined in chapter 4 where the inductance versus the distance of the target to the coil is examined.

Finally using the *Magnetic and Electric Fields* (mef.L11) module in COMSOL, the self-inductance of the coil was calculated to be 71.843 nH and 56.637 nH for square and circular coil geometries, respectively. These values were compared with those obtained from Equation 22 in chapter 2. The results obtained from both methods are shown in Table 3. As depicted, the results from the Equation 22 are well in agreement with what was obtained via the COMSOL simulation.

The simulation was repeated with a higher input current of 100 mA to compare the effect. The result of the simulation is also tabulated below. As shown in the Table 3, the magnetic flux density increases by a factor of 10 in value as current increases tenfold.

Table 3: Simulated magnetic flux density and the inductance at the center of the micro-coils. The calculated inductances using Equation 22 are also presented for comparison.

Geometry	Inductance from Simulation (nH)	Input Current (mA)	Magnetic Flux Density at Center (uT)
Square	71.843	10	99.7
Circular	56.637	10	82.4
Square	71.843	100	997
Circular	56.637	100	824
	Calculated inductance via Equation 22 (nH)		
Square	67.8		
Circular	56.8		

2.4. Detection Circuit and Software Algorithm

In this section, the signal acquisition circuit that is used to measure the oscillation frequency of the resonator is presented. We also discuss the custom software and algorithm that was designed and implemented from scratch -- in particular, the frequency counter function that measures the oscillation frequency of the sensors in the array. Next, we discuss how to expand the 2×2 sensor array by utilizing analog multiplexers. The proposed method allows for multiple resonator circuits to be connected to a single input on the microcontroller. Multiplexing the many signals coming from the sensor array is expected to save I/O pins, and be both space and cost effective. This should allow an entire array of touch sensors to be controlled with a single low-cost microcontroller.

2.4.1. Electric Circuit

As long as the Equation 14 (in Section 2.1.3) is satisfied, the resonant frequency can be approximated using Equation 8. The resonant frequency and the inductance are inversely proportional, and hence any changes in the inductance will change the frequency of the sensor's LC oscillator. The electronic read-out circuit works by measuring the resonant frequency and calculating the inductance based on the known capacitor value. By implementing a frequency counter and monitoring changes in the

inductance of the coil, we can detect variations in inductance caused by the user's touch on the touchpad and the deflections of the target diaphragm.

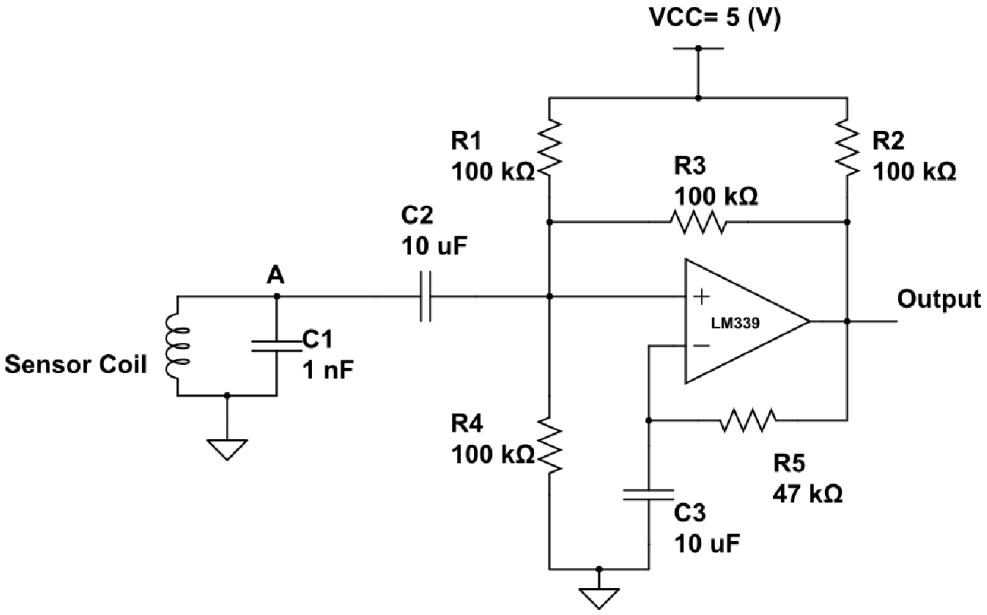

Figure 2.9: Detection circuit consisting of an LC oscillator containing the sensor coil, and a voltage comparator that allows for the measurement of oscillation frequency by a microcontroller [28], [46].

As shown in Figure 2.9, the first stage of the detection circuit is the LC circuit, consisting of the sensor coil and the high precision capacitor [30]. This stage of the detection circuit is slightly different for the binary switch compared to the eddy current sensor as will be explained shortly. In order to measure the oscillation frequency, a frequency counter was implemented using an Atmel® ATmega328 microcontroller. The Atmega328 utilizes an architecture that is optimized for low power and high-speed connectivity which means at 25ºC and 1MHz only uses 1.8V and 0.2mA in active mode.

The output of the LC circuit is an analog sinusoidal signal with frequency *f* as described earlier in Equation 9 in Section 2.1.2 Connecting an analog signal directly to the microcontroller requires an analog to digital conversion (ADC). Although it is possible to directly connect the signal to the microcontroller, it is undesirable to do so because this method requires using the microcontroller's onboard ADC. Since continuous monitoring of the signal is required in order to correctly detect the user's touch in real-time, several samples in each period of the sinusoidal signal are required in order to

correctly calculate the frequency. The microcontroller's onboard ADC is computationally costly and therefore was determined to be not able to meet the conversion timing requirement, resulting in a lower number of samples per period, which in turn leads to a lower resolution and therefore miscalculation of the frequency. To overcome this problem, a voltage comparator was used. Figure 2.9 shows that the output of the LC resonator is fed to an LM399 voltage comparator.

The LM339 is a low power quad voltage comparator that operates at 1.4mW when used with a 5 V supply voltage and is used to convert the sinusoidal signal into a periodic square wave with the same frequency as the LC resonator. This new square signal, which oscillates between 2.5 V and -2.5 V, can be directly fed into a digital pin of the microcontroller; the frequency counter then uses the built in edge detector to count the number of oscillations in a period of time, in order to calculate the resonant frequency.

The detection circuit used for the eddy current sensor, shown in the Figure 2.9, was modified slightly in order to be used for the binary switch. Because of the relative high resistivity of the conductive composite polymer compared to copper (which also leads to a smaller inductance), the LC resonator would be overdamped if the eddy current detection circuit were used as-is. In order to prevent this, a 120μH inductor L_1 was placed in series with the inductor coil L_X, forming an equivalent inductor L_2 as shown by Figure 2.10. This new and much bigger equivalent inductor allows the LC circuit to resonate.

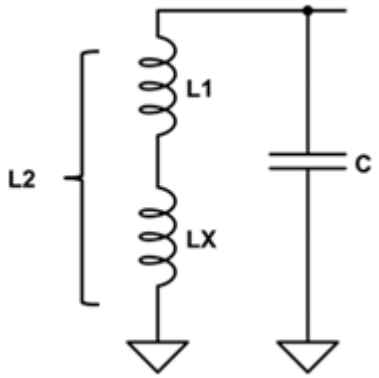

Figure 2.10: A series inductor L_1 was placed in series with the inductor coil L_X, forming an equivalent inductor L_2.

It is important to note that when there is an added resistance in a parallel LC circuit, there is a tendency for the added resistance to skew the resonant frequency. If the resistance is in series with the inductor, the resonant frequency shifts down; if the resistance is in series with the capacitor, the resonant frequency shifts up. This is called antiresonance. Because of the shift in the measured frequency, the resulting inductance values will be shifted as well and therefore do not show the real inductance values. It is important to note that this does not pose a problem in the functionality of the system, as the factor that determines the touch is the change in the inductance and not its initial value. As the change in the frequency and the inductance is preserved when dealing with antiresonance phenomenon, the detection system ignores the internal resistance and the inductor coil is treated as ideal. To calibrate the system, first L_x is removed, L_1 is shorted to the ground, and the resonant frequency is measured. The inductance L_x is then calculated using the following set of equations:

$$f_1 = \frac{1}{2\pi\sqrt{L_1 C}} \;\Rightarrow\; L_1 = \frac{1}{C(2\pi f_1)^2}, \qquad \text{Equation 23}$$

$$f_2 = \frac{1}{2\pi\sqrt{L_2 C}} \;\Rightarrow\; L_2 = \frac{1}{C(2\pi f_2)^2}, \qquad \text{Equation 24}$$

$$L_x = L_2 - L_1 = \frac{1}{C(2\pi)^2}\left(\frac{1}{f_2^2} - \frac{1}{f_1^2}\right). \qquad \text{Equation 25}$$

The remaining part of the detection mechanism circuit is identical to the eddy current sensor's circuit. The output of the voltage comparator is connected to the microcontroller, where the frequency counter monitors the change in the frequency of the sensor coil. Based on previous values stored and pre-defined thresholds, the frequency counter then decides whether or not a touch has occurred. Figure 2.11 shows the sinusoidal and square signals generated at node A and the output respectively using an inductor value of 19.1 μH.

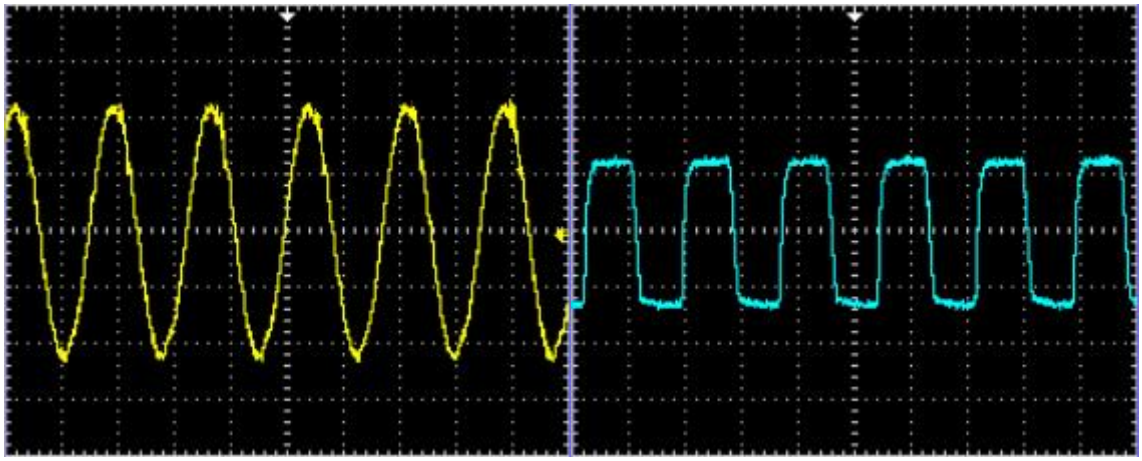

Figure 2.11: The LC oscillator creates a sinusoidal signal with a frequency of 1.15MHz at node A (200 mV/division) (Left). The output of the LM339 voltage comparator is a square signal with the same frequency as the LC oscillator that swings between 2.5 and -2.5 (V) (2V/division) (Right).

With the known capacitor value and the newly obtained frequency, the microcontroller calculates the inductance of the coil using Equation 9. The detection circuit based on this design was built and tested with known inductor values in the range of 500 nH to 200 μH. This range of inductance was chosen for testing based upon expected values of fabricated coils. The detection circuitry as-built was capable of accurately measuring the inductance of these known inductors with an error of ± 5%.

2.4.2. Frequency Counter Function

For measuring the oscillation frequency of the LC circuit, a frequency counter library called “FreqCount” by Stoffregen [47] is employed. FreqCount runs on the ATmega328 microcontroller; it takes a digital periodic signal as input and outputs the measured frequency. It measures the number of cycles that occur during a given time interval, and can best handle frequencies between 1kHz to 5MHz. It counts the number of oscillations of a periodic signal during a given time interval, and calculates the frequency based on that. When used at lower than 1kHz frequencies, fewer cycles are counted which results in less accurate measurements. For frequencies higher than 5MHz, the measurement takes longer than the timing requirement imposed by the high frequency signal and therefore the results would be incorrect. As a result of these limitations, when designing the oscillator system, it is crucial to select design parameters accordingly so that the resonant frequency falls into the supported frequency range.

When connecting the input signal to the microcontroller, the input must be large enough to drive the microcontroller’s input logic level; otherwise, an extra stage of amplification is required. We ensure that no additional stage was required by using the LM339 voltage comparator where the output was switched between 2.5 and -2.5V.

FreqCount library uses a timer interrupt to keep track of sampling time interval, and therefore interrupts were enabled when implementing the software. Other libraries that disable the interrupts temporarily or use the interrupt can cause incorrect results. If the hardware or any other program triggers an interrupt during the sampling time, it leads to a shorter time interval in which the measurement is taking place, counting fewer cycles while accounting them for the original time interval and therefore calculating an incorrect frequency.

Some of the important library functions used to implement the frequency counter algorithm for this project include:

(1) **FreqCount.begin(timeInterval)**: Starts the frequency counting operation. Input parameter “timeInterval” defines the sampling time interval, and is in milliseconds. We used 1ms time interval for this application because the

resonant frequency is in the range of tens of KHz, and this would give sufficient samples to calculate an accurate frequency.

(2) **FreqCount.end():** Stops frequency counting operation. After calling the function interrupts and analog write functionality can be used again.

(3) **FreqCount.available():** Returns *True* when a measurement is completed.

(4) **FreqCount.read():** Returns the most recent measurement. Since the measurement is buffered, it must be read first before another measurement can be made.

The Atmega328 microcontroller has three timers on board that can be used for generating PWMs, counters and timers. The *FreqCount* Library utilizes two timers: *Timer/Counter1* counts the number of events that cause a rising edge on the input digital pin and *Timer/Counter2* that keeps track of the time interval in which the measurement is taking place. The frequency counter starts by first zeroing the counter values and resetting both Timer/Counter1 and Timer/Counter2. Timer/Counter1 is set to counting mode and Timer/Counter2 is set to Clear Timer on Compare (CTC) mode. With a 16 MHz clock running the Atmega328, every clock tick is 62.5ns long. With a pre-scale of 128, every increment on the Timer/Counter2 represents 8μs. Therefore, in order to reach a time interval of 1ms, Timer/Counter2 needs to count to 125.

The function then runs until an interrupt is asserted, at which point the 16-bit counter register value (TCNT1) is read and stored. Then, the time elapsed is checked with the Timer/Counter2 to check if the end of the time interval has been reached. If the specified time interval has been reached, the counter value is added to the total count number, simultaneously adding any possible overflow to the total count number where each overflow represents 2^{16} = 65536 counts. Finally, the *result_ready* flag is set to show that the measurement has been completed. Otherwise, if the time interval has not been reached, the counter value is added to the total count number, the interrupt is acknowledged and the operation continues until another interrupt is asserted.

2.4.3. Coil Readout Scheduler Module

At power up, the system measures the reference coil's inductance by calling the FreqCount library. The inductance value is stored and used to calculate and set threshold values based on user defined parameters. After the initial setup, the system enters a scheduler at which time it loops through the sensor coils one by one, measuring their inductance and comparing the percentage change in the inductance values with the threshold value to determine if a touch has occurred. If the change in the inductance exceeds the defined threshold value, a flag is set to show that a touch has been registered. Sampling of the coils continues until the stopping condition is triggered by the user, which is defined as pressing a push button on the microcontroller board. Figure 2.12 and Figure 2.13 show a simplified flowchart of the coil readout scheduler module and frequency counter module, respectively.

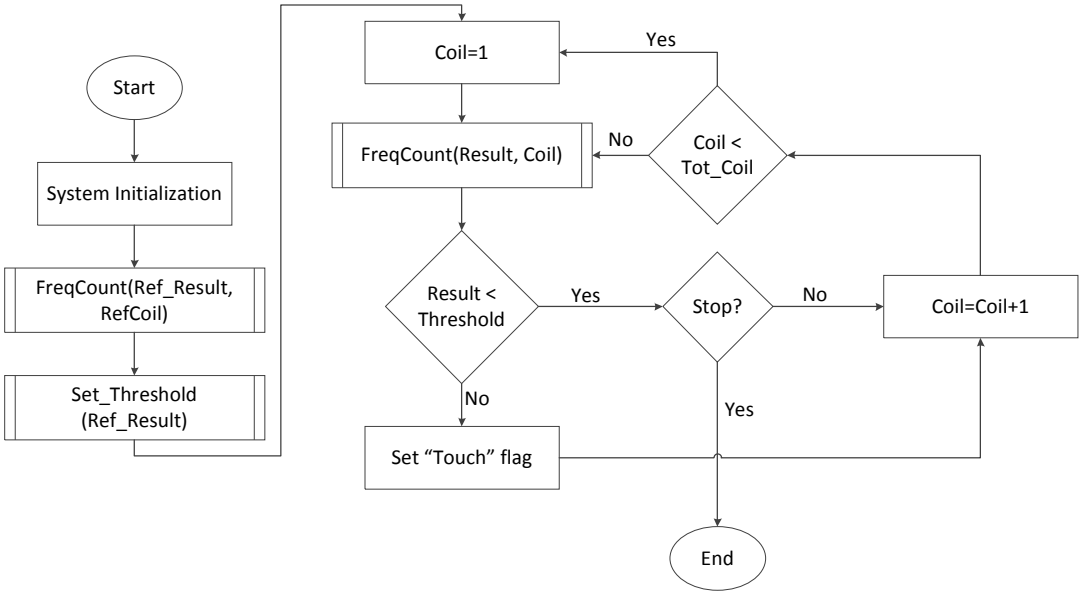

Figure 2.12: Simplified Flowchart of the coil readout scheduler algorithm used in the detection system.

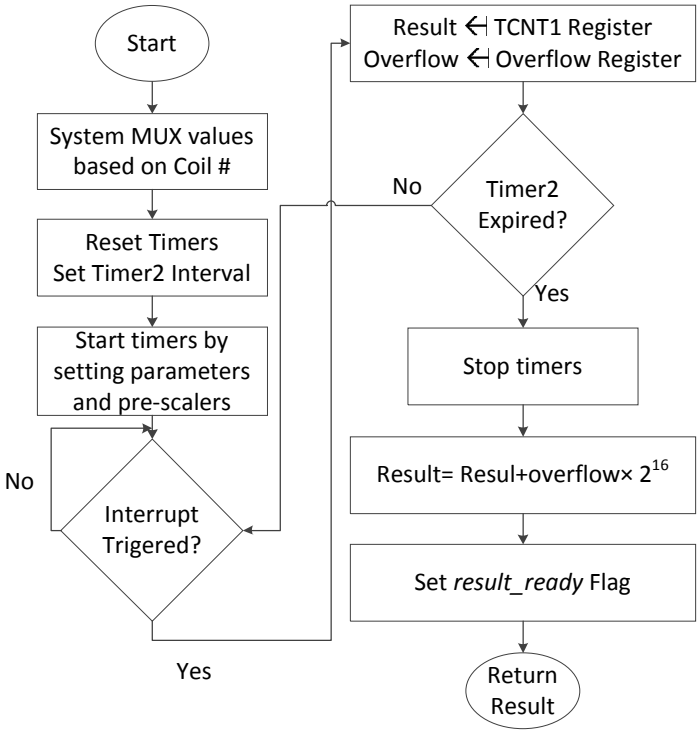

Figure 2.13: Simplified flowchart of the frequency counter algorithm used in the detection system.

2.4.4. System Power-Up

As mentioned previously, at power-up, the system scans all of the connected sensors and measures their corresponding inductance values. These values are stored for averaging, calculating threshold values, and for later comparison to determine if a touch has occurred. As a result, at power up all the touchpads must be un-pressed so that the measured inductance values reflect the “initial” or undisturbed numbers. An alternative approach would be to use a reference coil, whose inductance is independent of user interactions, to obtain the initial values. Using this method, the inductance value of the reference coil can be used for averaging and calculating threshold values. Implementing this method is simpler than the former, however in the testing and characterization of the device because each senor unit was to be tested rigorously and independently of the others, the use of reference coil was disabled in the software.

2.4.5. Use of Analog Multiplexer to Optimize and Expand Sensor Array Design

The LM339 consists of four independent voltage comparators that can be connected to four LC oscillator circuits, resulting in a 2×2 array. An analog multiplexer is used to connect multiple sensing coils to a single capacitor. The multiplexer ensures that each coil is electrically insulated from the others, and that only one coil is part of the LC oscillator at a time. The insulation of parallel sensing coils is done by controlling the selection lines of the analog multiplexer through microcontroller's GPIO based on the firmware commands. Figure 2.14 shows an array of coils arranged for a multiplexer-based system.

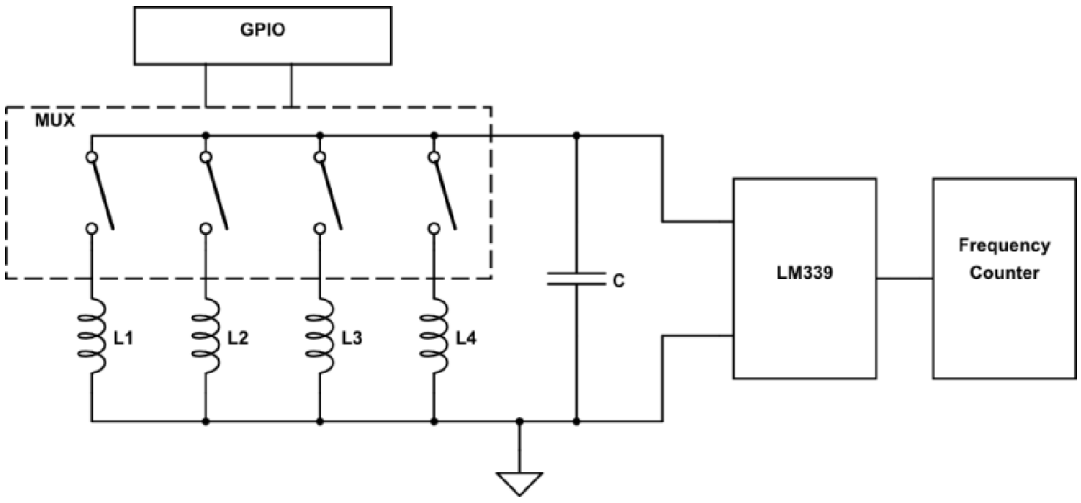

Figure 2.14: An array of sensor coils arranged for a multiplexer-based system connected to a single capacitor all controlled by GPIO's coming from the microcontroller allowing to create a larger array of sensors using a single LM339 voltage comparator.

The switching rate at which the coils can be selected depends on a variety of factors. The frequency counter in the microcontroller must have finished measuring the oscillation frequency before a new coil can be replaced. Therefore, when designing the oscillator in order to minimize the measurement time, the capacitor value must be chosen such that the oscillation frequency is as fast as possible.

In order to accurately measure the frequency of the oscillation, the frequency counter function was written in such a way that it measures the number of oscillations during an interval of time, and based on that calculates the resonant frequency. A longer time interval allows for more measurements and therefore more accurate frequency calculation. For an array of four sensors with a resonant frequency in the kHz range, we set this value to be 1 ms. However, this value can be smaller for a larger array of sensors, to allow a faster switching between the sensors. By altering the value of the capacitor, the resonant frequency can be set to be in the mega-Hertz range to accommodate for this. In addition, the analog multiplexer itself adds an extra delay when switching inputs. For switching between four coils, the CD4052B analog multiplexer by Texas Instruments was used. Based on the CD402B's datasheet, with a slew rate of 20 ns, it takes approximately 25 ns for the output to stabilize when switching between the inputs. This transition delay was taken into account in the software by adding extra software delays to ensure that the output signal was stable before frequency measurements were performed. In the firmware, since a 16MHZ clock is driving the microcontroller using a NOP (no operation) statement, a minimum delay possible of 62.5 ns was added before frequency counter function was called.

The CD4052B analog multiplexer uses break-before-make switching, which electrically isolates coils from one another and therefore eliminates interference between the coils. Also, the analog multiplexer has a low dynamic power dissipation of 100 μW at a 10 kHz switching frequency when powered with 10 volts (Vdd=10V), which is ideal for low power electronics and applications. It also has low ON impedance, which means that it doesn't change the oscillation frequency of the resonator. The ATmega328 microcontroller provides a limited number of digital inputs and therefore the number of LM339's that can be connected directly to the microcontroller is also limited. In a similar approach to what was explained above, we have been able to multiplex the LM339 so that each input of the microcontroller can also be connected to four LM339's.

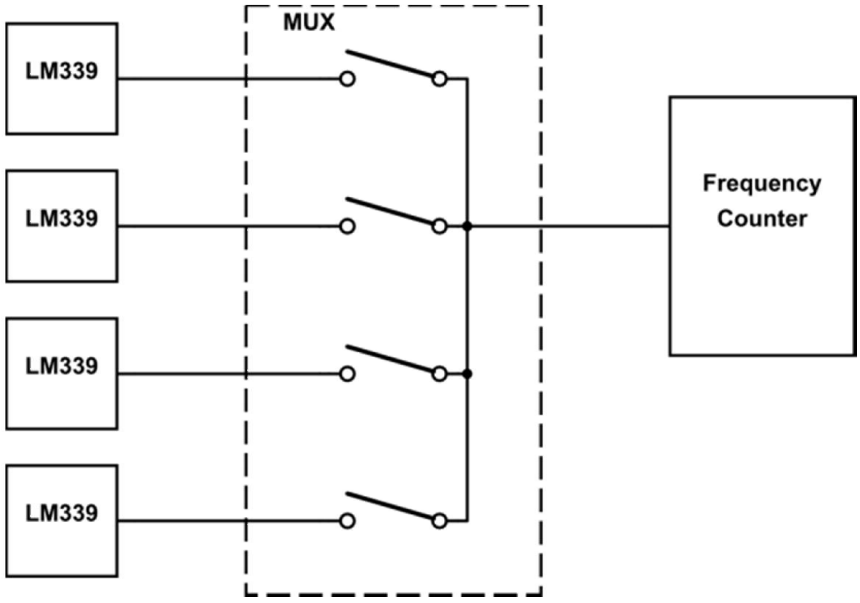

Figure 2.15: Four LM339 voltage comparators connected to a single frequency counter controlled by the microcontroller GPIOs, which allow the creation of a larger array of sensors using a single frequency counter.

Figure 2.15 shows how four voltage comparators are connected to a single frequency counter input of the microcontroller. Using this approach, we are able to connect 16 switches, all controlled by four control signals from the microcontroller. Controlling the selection lines is done on the firmware side of the microcontroller. The implementation of the system is straight-forward, as the sensors are being read sequentially. Appropriate delays were added between each reading to ensure the oscillator signal has stabilized when switching between sensor coils. In order to prevent inconsistencies in the measurements that could occur due to cross talk between the sensors, variation in drive current or temperature changes (small variation in inductance due to thermal expansion or contraction of the coil and change in resistance), the reference coil was used. The reference coil needs to be identical in size and shape to the sensors coils to have the same inductance, with the only difference being a non-moving target. The readings from the sensor coil are normalized by calculating the ratio of the inductance of the sensor coil to the reference coil. Any variations in the system that are not induced by the user will affect both the sensor coils and the reference coils the same way, and result in a ratio of one. By normalizing the readings, the variations fall out and what is left in the measurement reading is the effect of the user interaction.

Another standard method to achieve the similar result is the use of ratiometric measurement where a reference coil is placed in series with the sensing coil and is driven by the same current. In our earlier system design iterations where the sensing parameter was the change in the impedance, this method was used. The voltage measurement was reading a ratio of the two impedances and therefore would give a normalized value. Figure 2.16 shows the reference and the sensor coil configuration in ratiometric measurement.

In terms of total power dissipation, we estimate that, by adding up the power dissipation of the PCB coil and all electronics, the total power dissipation to be less than 10 mW.

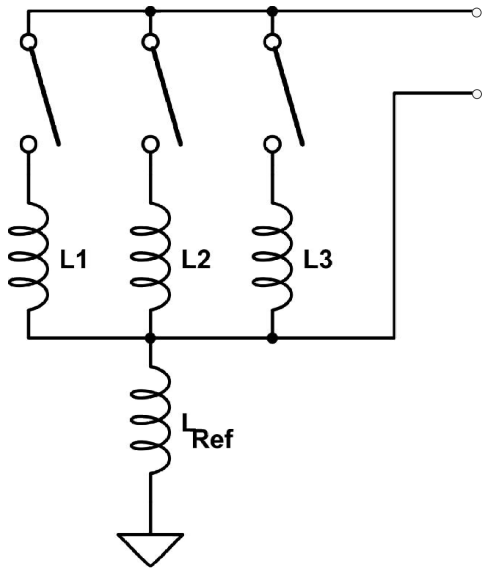

Figure 2.16: Ratiometric measurement of the inductance using a reference coil L_{Ref} that is placed in series with the sensing coil. Any variations in the system that is not induced by the user will affect both coils the same way and will be ignored in the measurement.

Chapter 3.

Fabrication

This chapter describes the fabrication of the sensors using different techniques for the inductive sensors. The first describes a technique for patterning two-layer inductive coils on flexible PCBs. Next, a fabrication technique that uses PMMA as a mold to create a conductive flexible target by embedding copper film in PDMS is described. Finally, the details of fabricating coils along with their corresponding target structure using conductive composite polymer (CCP) or thin metal film embedded in PDMS are presented.

3.1. Fabrication of PCB Coil Sensor System

Figure 3.1 summarizes the fabrication process of the double-sided coil on a double-sided flexible PCB board held together by epoxy . Fabrication of the PCB coils was performed using standard photolithography and PCB etching methods. Photomasks were design using Tanner EDA L-edit, a microelectromechanical systems (MEMS) layout editor. Several photomasks with several coil structures that differed in dimension, geometry and coil parameters such as number of turns were drafted. These photmasks were printed at Samco Printers Ltd, a local commercial printer in Vancouver, BC. The print shop has a resolution of 1016 dpi and is theoretically capable of printing structures as small as 10μm. All the designs were converted from standard GDSII format into Portable Document Format (PDF-Mask) prior to sending them to the print shop. Micro-size imperfections due to the printing process between the opaque and transparent sections were observed, however, since the coil structures were much larger than the maximum resolution available, these imperfections did not cause any problems in the fabrication process.

In order to prepare the substrate for photoresist coating, first the substrate was cleaned to ensure a uniform distribution of the photoresist. The flexible PCB was first dipped in an IPA bath for 5 minutes in order to remove any surface contamination. Next, both layers of the PCB were first rinsed with acetone and then with running DI (Deionized) water for 3 minutes. The PCB substrate was then dried by blowing dry nitrogen on it to remove any water droplets from the top and bottom layer. To ensure the substrates were completely dehydrated, they were baked at 100 °C for 20 minutes in a soft bake oven.

A variety of photoresists can be employed for the patterning process. Considering availability and cost, the Rohm & Haas S1813 positive photoresist was used. In order to coat the sample, we used direct a spin-on technique. A volume of 3-4 droppers-full of the photoresist was placed at the center of the front layer of the sample and spun at 3000 rpm for 30 seconds to achieve a uniform distribution. In order to spin-coat the bottom layer, the top layer was placed on the vacuum chuck. To prevent any blemishes on the photoresist, the sample was first soft baked for 10 minutes at 100°C. Any longer baking time should be avoided since the bottom layer also requires a soft baking step which could cause “over-baking” of the photoresist that would lead to difficulties in removing it during the development stage. After this quick soft bake, the bottom layer was then spin coated with photoresist in a similar way as to the top layer. Extra care was taken at this stage to avoid damaging the top layer’s photoresist

Following the spin coating, in order to condense the photoresist and ensure the coating’s adhesion to the substrate, the sample was soft baked for 20 minutes at 100°C [48]. The use of a hot plate is not recommended because the high heat conductivity of copper causes the photoresist to “burn” at the point of contact between the sample and the hot plate. After cooling, the sample was placed in a mask aligner (Quintell 4000) and the front layer was exposed to the pattern on the photomask using i-line UV-light with a wavelength band of 365 to 405 nm for 30 seconds. Following exposure, the sample was bathed in the photoresist developer solution MF319 (by Microposit) with slight agitation to ensure that the dissolving photoresist was quickly removed from the reaction site. The development time used was approximately 60 seconds, but depends on the photoresist’s exact thickness, agitation and feature sizes. The endpoint of the process

was determined by eye. By using a positive photoresist with a dark film mask the regions of the photoresist not covered by the mask were exposed and dissolved in the development stage. After development, the sample was immediately rinsed under running DI water for 3 minutes and then dried. Next, it was hard baked at 120° C for 20 minutes in preparation for the etching process and for increasing photoresist adhesion.

In the next step, the sample was placed in a bath of copper etchant (Ferric Chloride solution provided by M.G. Chemicals Ltd.) that was heated to 50°C to help speed up the etching process. The Ferric Chloride solution is highly corrosive and must be handled with extreme care and was performed under a fume hood with appropriate safety precautions. The etching process took about 10 minutes and the process endpoint was determined by eye. Careful inspection was required to prevent over-etching of the structures since, when the etching reaction between the copper and the etchant starts, the etchant's color changes into a dark black color which practically hides any structures underneath. Before continuing to the next step, the remaining resist was removed from the sample. The sample was then placed in acetone for 5 minutes and then rinsed with DI water.

In order to pattern the bottom layer of the structure, this entire process was repeated. For patterning the bottom layer, the steps are all similar to the ones explained above, except that in order to prevent etching the newly made structures on the top layer, it was coated with a thick (300 μm) protective layer of photoresist. Since the flexible PCB is not transparent, in order to properly align the top and the bottom layer, a small through-hole was made at the center of the connection pads of the coils on each side as a visual aid. This through-hole was later used to connect the top and bottom layers of the coil. At the end of the patterning process, the entire remaining photoresist layer was stripped using an acetone bath. Finally, in order to make the electrical connection between the top and bottom layers, the through holes were filled by CW2460, a two part conductive epoxy by CircuitWorks®, and left to fully cure for 5 hours.

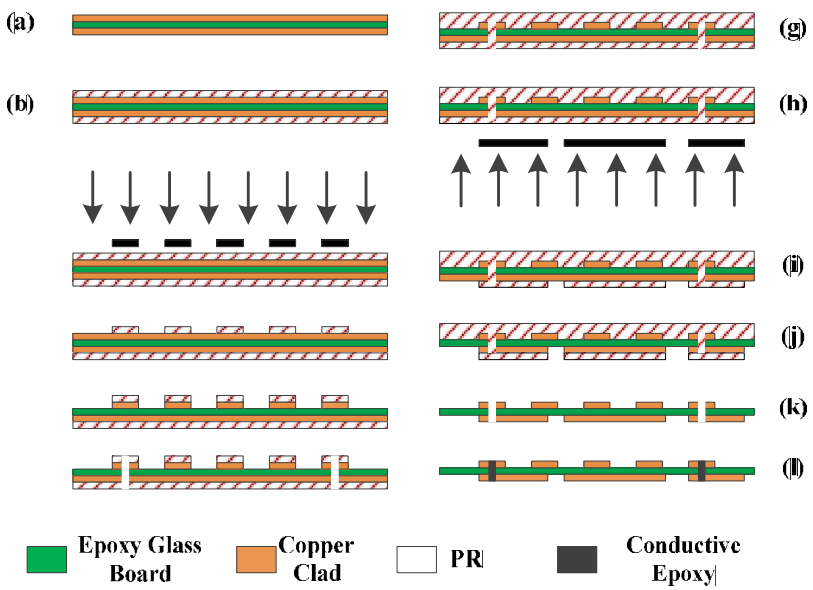

Figure 3.1: **Fabrication steps for patterning the coil on a double-sided flexible PCB: (a) double-sided flexible PCB; (b) spin coating of photoresist (PR) on the top and bottom layers of the flexible PCB; (c) exposure of the top layer of the flexible PCB; (d) developing PR; (e) pattering the flexible PCB copper layer (top); (f) drilling connection through-holes and alignment marks; (g) spin coating a thick protective PR layer on the top layer of the flexible PCB; (h) exposing the bottom layer of the flexible PCB; (i) developing PR; (j) pattering the copper layer of the flexible PCB (bottom) ; (k) stripping the PR; (l) filling the connection holes with conductive epoxy.**

3.2. Fabrication of Polymeric Coil Sensor System

With the use of photolithography techniques that have been perfected for the semiconductor industry, microfluidic and MEMS devices can be fabricated using silicon substrates with proper surface finishing. Furthermore, in recent years, polymer based devices have become more and more popular in the microfluidics and MEMS fields for a wide variety of reasons. Complicated and time consuming fabrication techniques (such as etching, drilling, etc.) that are required for silicon, glass, as well as regular and flexible PCB, can be minimized when using these newer polymer-based systems. A variety of polymers have been employed, with polydimethylsiloxane (PDMS), poly(methyl methacrylate) (PMMA), polycarbonate (PC), polyimide (PI), poly(styrene) (PS) and poly(ethylene terephtalate) (PET) are among the most popular ones.

As mentioned previously, PDMS has many favorable characteristics including: low cost, ease of fabrication via micromolding and soft lithography, ease of sealing and mechanical compliancy [31]. PDMS is a well-researched silicon-based elastomeric thermosetting polymer, widely used in microfluidics and microelectromechanical systems (MEMS) and was chosen for this project because of its many favorable characteristics. PDMS can be patterned using a variety of methods, with micromolding being the most common. Among all the aforementioned polymers, PMMA is an excellent choice for micromolding masters for PDMS due to its low cost, wide availability, biocompatibility, high chemical inertness and mechanical strength [31], [49]. For example, PMMA can be used in LIGA (Lithography, Electroplating, and Molding) to fabricate high aspect ratio microstructures structures [50]. PMMA sheets are available at different size and thicknesses and can be cut into desired dimensions for other applications for use as a mold or substrate. When used as a mold, the thickness of the PMMA used is determined by the ablation depth required for the structure. For the fabrication of the polymeric coil and the sensor interface presented in this thesis, CO_2 laser ablation, a low cost micromachining method for creating micromolds, that has been used at Microinstrumentation Laboratory over recent years was employed.

For the fabrication of the molds employed in this thesis, we used the Universal Laser System's VersaLASER© which operates at a maximum power rate of 60 watts

and can produce an invisible laser beam at wavelength of 10.6 μm. The system can operate at both vector and raster modes to produce different shapes. For this work, the raster mode was used to ablate structures on the PMMA sheets with thickness of 1/8 of an inch. Since the system can operate at different power and speed settings, it is required to pre-calibrate the system in order to achieve the desired structure depth. The structures were drawn using CorelDRAW Graphics Suite, a computer-aided design (CAD) program, and then transformed to G-code using Laser Interface+™ software, a laser print driver for material processing systems that is also supplied by Universal Laser System. The "Print function" generates the G-code based on the design and sends these commands to the laser system where the laser intensity and motor movements that determined the location of the beam was controlled. A CO_2 laser beam ablates the PMMA photothermally in which the focused laser beam light is absorbed and converted into heat, resulting in melting and vaporizing the PMMA target spot. When laser beam meets the PMMA sheet, as the temperature rapidly increases, because of PMMA's high absorptance coefficient and low heat capacity and low heat conductance, the irradiated spot melts rapidly and evaporates [50].

Once the molds were created, the structures were fabricated by casting conductive composite polymer (CCP) and PDMS on the laser-cut PMMA mold. The sensor coil is a double sided structure and therefore required two separate molds, one for each side. The two sides were fabricated separately, and then bonded using plasma surface activation to achieve a double-sided structure. The overall fabrication process for each side is summarized in Figure 3.2. FL45 is a two-part silver based conductive composite polymer that consists of base silver composite and a curing agent (purchased from Zoflex®,USA) that was used as the conductive material to create the coil and also was one of the materials the was used to create target structure. The two parts were mixed in a ratio of 6.63 to 1. With a volume resistivity of 0.2 Ω.cm and shore A hardness of 45 (according to company data sheets), FL45 is highly conductive and is quite soft, and results in a flexible structure once cured.

The fabrication process for each segment follows the same subsequent procedure and starts with casting the conductive composite polymer first. The base conductive polymer and the curing agent were mixed at a ratio of 6.63:1 as

recommended by the manufacturer. First, the prepared conductive polymer was applied on the mold and the excess was scraped using a glass squeegee, resulting in the conductive polymer only filling the engraved cavities in the mold that later became the coil, connection traces or other desired structures. In the next step, the PDMS was prepared. Polydimethylsiloxane (PDMS) (Sylgard 184 Elastomer Kit) purchased from Dow Corning, USA, consists of a base elastomer and a curing agent and were mixed at a ratio of 10:1 as suggested by the manufacturer. The mixed solution was degassed in a vacuum chamber. Next, the mix was poured over the mold to cover the conductive structures and create a 1 mm to 1.5-mm-thick layer and left to bake at 100 °C for three hours to fully cure. During the curing process, the FL45 and the PDMS physically bonded together to form a single structure. Following curing process, the structures were carefully demolded. For the sensor coil, this process was repeated for each side of the coil and the two layers were bonded together.

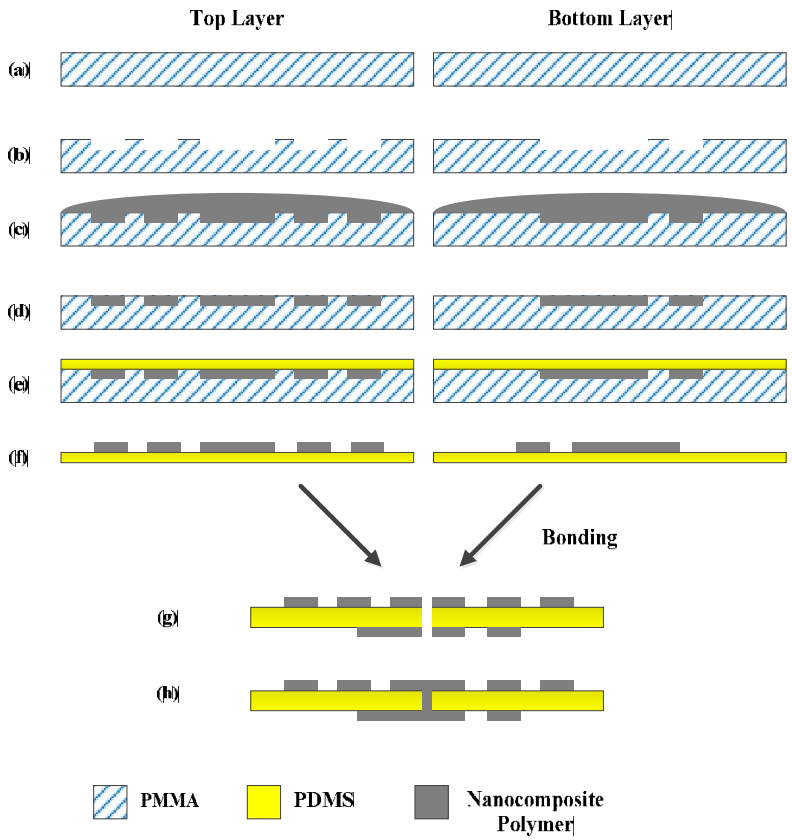

Figure 3.2: Steps of the microfabrication process for composite polymer coil: (a) PMMA sheet; (b) pattering of the PMMA mold using Universal Laser System's VersaLASER© CO2 Laser ablation system; (c) filling the mold with composite polymer; (d) removing excess composite polymer; (e) casting PDMS; (f) demolding; (g) bonding of the top and bottom layers and punching a through hole for electrical connection of the two layers using a 15 gauge dispensing needle; (h) filling the through hole with composite polymer to connect structures on the top and bottom of the two-sided device [28].

Bonding the two layers was achieved using plasma surface activation using a hand held corona device (model BD-20AC from Electro-Technic Products Inc., Chicago, USA). Each sample was cleaned thoroughly using IPA to remove any contaminations that were present on the surface and then placed on a clean glass surface on top of a non-conducting surface. The corona generates a high-voltage potential above the sample's surface which ionizes the surrounding air and creates a localized plasma, resulting in the activation of the PDMS surface. Considering the size of the samples, a 3-inch filed effect electrode was chosen for this application. The electrode was moved back and forth approximately ¼ inch above the bonding surface of each layer for about

40 seconds. The two layers were then immediately brought into contact and pressed together to permanently bond them. The top and bottom layers were aligned such that the center of the coil on the top overlapped the connection pad on the bottom layer. The sample was left undisturbed for one hour for the bonding to complete. Figure 3.3 shows the experimental setup for bonding the two layers using plasma surface activation [51], [52].

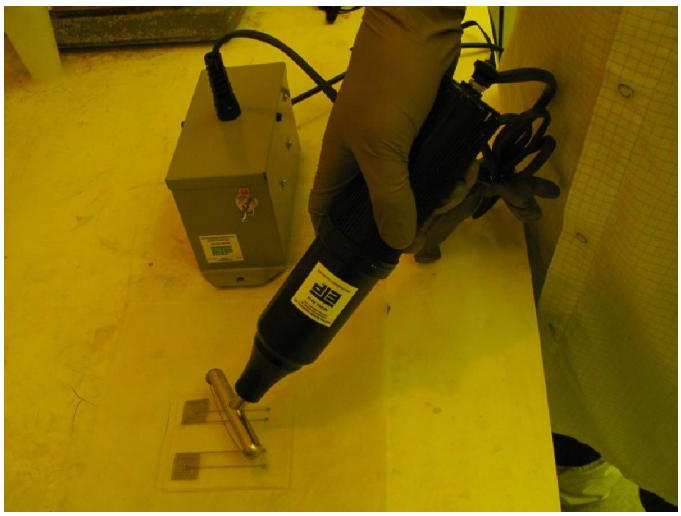

Figure 3.3: Experimental setup for bonding a two-layer PDMS substrate together using the corona surface activation device.

After completing the bonding, in order to create the electric connection between the top and the bottom layer of the coil, a 15 gauge dispensing needle was used to create a through-hole via punching the center of the coil on the top layer, penetrating the connection pad at the bottom layer. This hole was then filled with FL45 conductive polymer.

3.3. Fabrication Process for Creating the Interface Using Conductive Composite Polymer

The fabrication process for creating the interface segment of the system using conductive composite polymer uses the same techniques employed to create the polymeric sensor coil. The interface (fascia, target and the spacer) is a single structure that was fabricated using a single mold. Laser cut molds made of PMMA sheets were

used to create the structure. The fabrication process was done by casting CCP in a 25 mm by 25 mm square cavity (which fully covers the sensor coil) to form the conductive target. Later PDMS was poured over the CCP to create the spacer and the remaining parts of the structure. The sample was left undisturbed to fully cure. After the demolding and completion of fabrication of the interface and the sensor coil, the two components (coil array and the interface) were assembled together and bonded using silicone sealant to make a single structure. Figure 3.4 shows placement of the interface on top of the coils.

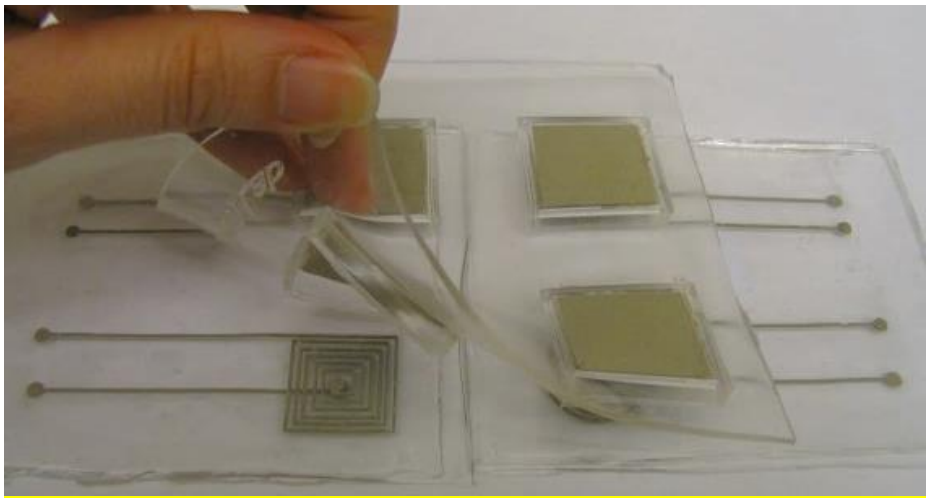

Figure 3.4: Placement of the interface on top of the coils. The two elements (interface and the coils) were bonded together using silicone sealant to make a single structure before the testing was done.

3.4. Fabrication Process for Creating Conductive Target by Embedding Copper Film in PDMS

The fabrication process for embedding copper film in PDMS uses the same techniques employed in the previous section with the exception that CCP is replaced with a thin copper film of a 0.005 inch thickness that is flexible and can be deflected by the user during movement of the interface. Because of the small thickness of the copper film, there was no need to design new molds for this process since the copper film can easily fit the square cavity contrived to house the conductive target. Figure 3.5 shows a summary of the fabrication process. The fabrication process starts by casting a small layer of PDMS on only the square cavity previously used for CCP. This thin layer of PDMS along with the top layer sandwiches the copper film and mechanically bonds it to the rest of the structures. The PDMS mixture was degassed in a vacuum chamber and left at 100°C to bake for three hours. Once the PDMS was cured, the thin copper film was placed on top of the PDMS at the center of the square cavity. The copper film needs to be cut 1 mm smaller than the actual square cavity on each side to allow the top and bottom PDMS layers come into contact and bond together during the second curing stage. Finally more PDMS was poured over the mold to fully cover the target structure and the spacer to create a 1.5 mm bonding layer connecting all the structures together, following a degassing and baking stage similar to the previous stage.

Figure 3.6 shows the fabricated interface by embedding thin copper in PDMS. The Interface was placed over the inductive coil and glued in place to create a single structure. Since the same molds were used in the fabrication of the interface as the one used in the previous method, all the dimensions remain the same.

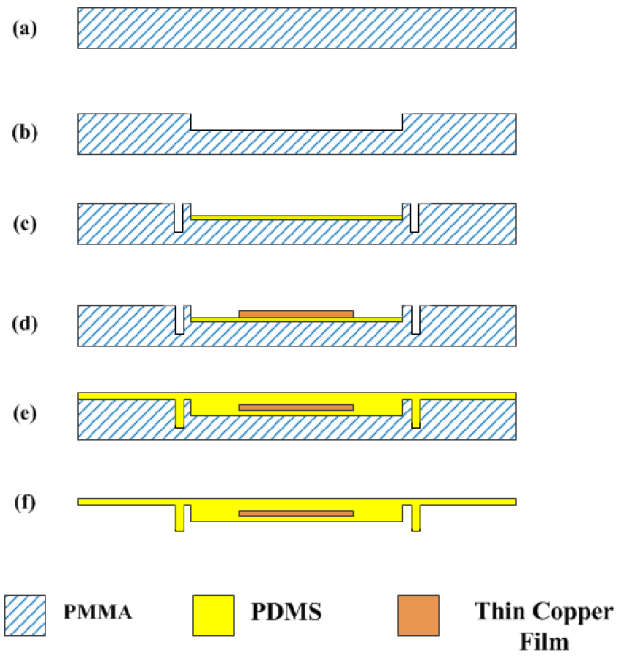

Figure 3.5: **Steps of the microfabrication process for creating a conductive target by embedding a thin flexible copper film in PDMS: (a) PMMA sheet; (b) pattering of PMMA mold using Universal Laser System's VersaLASER© CO2 Laser ablation system; (c) casing a thin layer of PDMS in the target cavity; (d) placing the thin layer of copper on top of the PDMS; (e) casting PDMS; (f) demolding.**

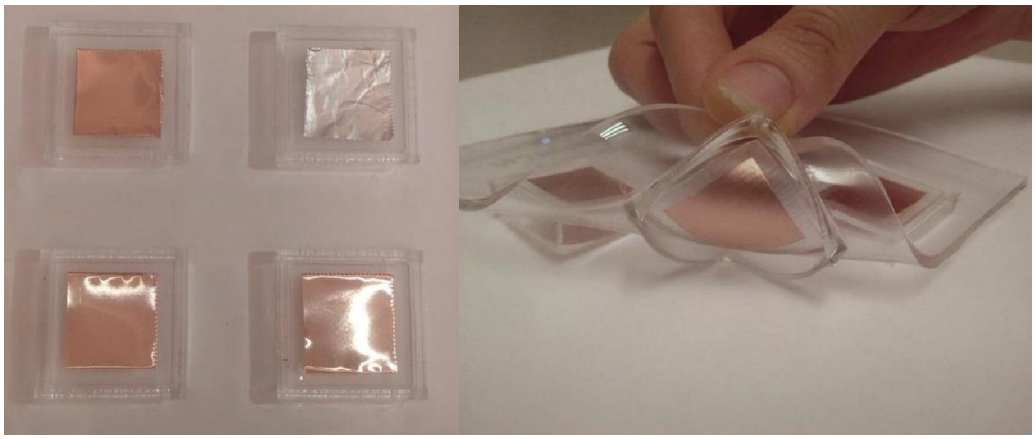

Figure 3.6: **Fabricated interface by embedding thin copper (reddish brown color) and aluminum (bright grey color) film in PDMS to create flexible conductive targets.**

Chapter 4.

Experimental Procedures and Results

In this chapter, the results for both types of sensors, eddy current and binary switch, are presented. First, the results of the fabricated eddy current sensors, along with the device characterization, are presented. Next, we describe the fabricated sensor coils made of CCP and explore the effects of the deflection on the internal resistance of a test structure as well as sensor coils. Finally we examine the effects of these deflections on the inductance of the coils.

4.1. Experimental Procedures and Results for PCB coils

In this section, results for the fabricated flexible Printed Circuit Board (PCB) metal sensor coils are presented, and the effect of generated eddy currents on the resonant frequency is studied.

4.1.1. Fabricated Eddy Current Sensor Devices Using Flexible PCB

Prototypes of the eddy current sensor coil arrays were successfully fabricated based on the techniques explained previously in Chapter 3. The fabricated coils on the flexible PCB had an outer diameter of 21 mm, with 20 turns and a trace line width of 200 μm and a line to spacing ratio of 1:1. Figure 4.1 shows the final patterned flexible PCB that consists of a 2×2 array of square and circular geometry sensing coils.

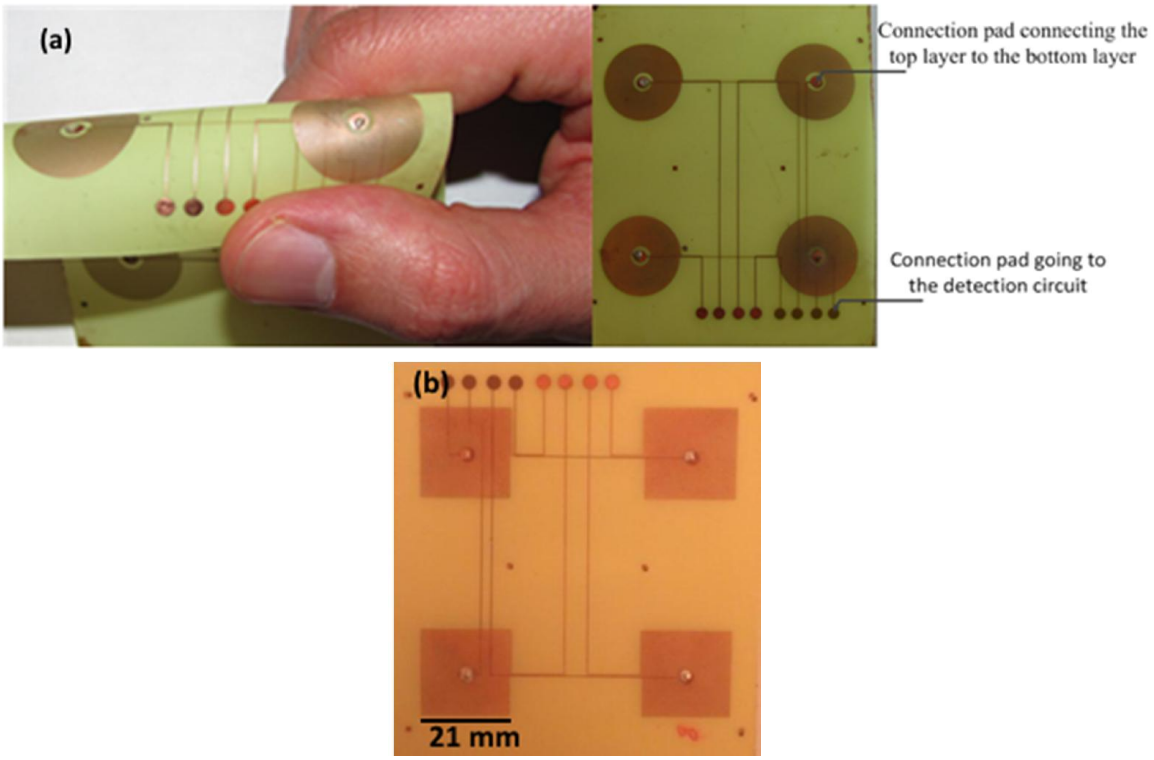

Figure 4.1: Patterned coil array on two layer flexible PBCs showing a 2×2 array of a) circular and b) square geometry sensing coils [28].

After the interface assemblies were placed over the coils, using designated connection pads on the designed PCB, the sensor array was connected to the detection circuit in order to measure the resonant frequency of the resonators. Since the LM339 chip contains four voltage comparators, each sensor unit in the sensor array was connected to an individual input of the chip.

The interface was designed such that, for each sensor, the spacer separates the target from the sensor coil by a distance of 5.5 mm, large enough to generate small eddy currents in the target. The resonant frequency of the four PCB coils was measured to be between 850 to 900 kHz for the circular geometry and 750 to 800 kHz for the square geometry with the presence of the interface. Base on the obtained values, the average calculated inductance for the four coils in the array was 33.1 ± 1.9 μH and 41.9 ± 2.1 μH for circular and square geometries, respectively, where the variation is one standard deviation. The deviation in the measurements can be attributed to the different lengths in the connection trace lines, discrepancies introduced by imperfections in the conductive

epoxy, as well as error in the measured frequency by the detection circuit. In addition, due to the positioning of the sensors in the array, over-etching or under-etching of the copper lines in different regions of the original copper plate during photolithography may cause variation in width and spacing, as well as in the conductivity of the structure, which in turn may introduce variations in the coils' inductance values.

It was observed that flexing the system changed the coils' inductance only very slightly. Since the changes in the inductance due to flexing the structure were small compared to when the switch was pressed (less than 5% of the original value), these changes was easily ignored by the detection software by setting a change threshold of at least 15%. The threshold values were optimized to only recognize a minimum of 15% change in the inductance as a user's touch to prevent false triggers caused by the bending of the coil.

It was observed that by applying pressure and causing the flexible membrane to bend toward the sensing coil, the resonant frequency increased, indicating a drop in the inductance of the coil due to eddy current generation. When the target was depressed fully and only separated from the coil by a thin 100 μm layer of PDMS, the measured frequency was 960kHz, which is 40% higher than its initial value. We fully characterize the resonant frequency of the inductor versus the distance between conductive target made of different materials in the next section.

4.1.2. Characterization of Distance versus Frequency Change in the PCB Coil

In this section, the fabricated square PCB sensor coils were examined (since they have the highest inductance for the area they occupy) to study the effect of generated eddy currents on the resonant frequency by changing the distance between the coil and the target. The PCB coils, along with different conductive materials, were used in this experiment to study the eddy current generation with materials that have different properties. For the conductive target in addition to the conductive composite polymer target, aluminum, copper and stainless steel were also studied. Table 4 shows the properties of these materials [53].

Table 4: Conductivity and Resistivity of the target materials used in characterization of distance versus frequency change in the PCB coil

Material	Conductivity (S/cm)	Volume Resistivity (Ω·cm)
Copper	5.85×10^{5}	1.7094×10^{-6}
Aluminum	3.69×10^{5}	2.71×10^{-6}
Cast Iron	1.01×10^{5}	9.901×10^{-6}
CCP	5	0.2

The distance between the coil and target was increased in steps of 500 μm increments to a maximum of 6 mm and the corresponding resonant frequency values were recorded at each angle for each conductive target. When copper, aluminum and cast iron were used as the conductive material, the effect of the eddy current generation when the target was in proximity of the coil was strong enough to increase the resonant frequency up to 40% of its original value. Figure 4.2 shows the resonant frequency versus distance between different conductive target materials and the fabricated square PCB coils averaged over the 4 samples in the array. As shown in the figure, the measured frequency for the cast iron is the lowest of the three conductive targets. Iron is a ferromagnetic material. As a ferromagnetic target approaches the coil, eddy currents are generated in the target and therefore the inductance is reduced. However, as the target approaches the target, the coil's core reluctance decreases because of iron's high permeability. The magnetic reluctance in the coil is analogous to electric resistance: magnetic flux is "reluctant" to travel thorough a material with high reluctance such as air. The decrease in magnetic reluctance will result in a higher flux through the magnetic coil and therefore will increase the inductance[54], [55]. These two effects are in opposite directions and therefore they cancel each other out. For our system, however, the effect of the eddy current in the change in inductance was greater than the effect caused by the reluctance. Thus, when the iron target was in proximity of the coil, similar to the non-ferromagnetic material such as copper, the overall inductance dropped. However, this drop was lower compared to what was measured for the aluminum or cooper target.

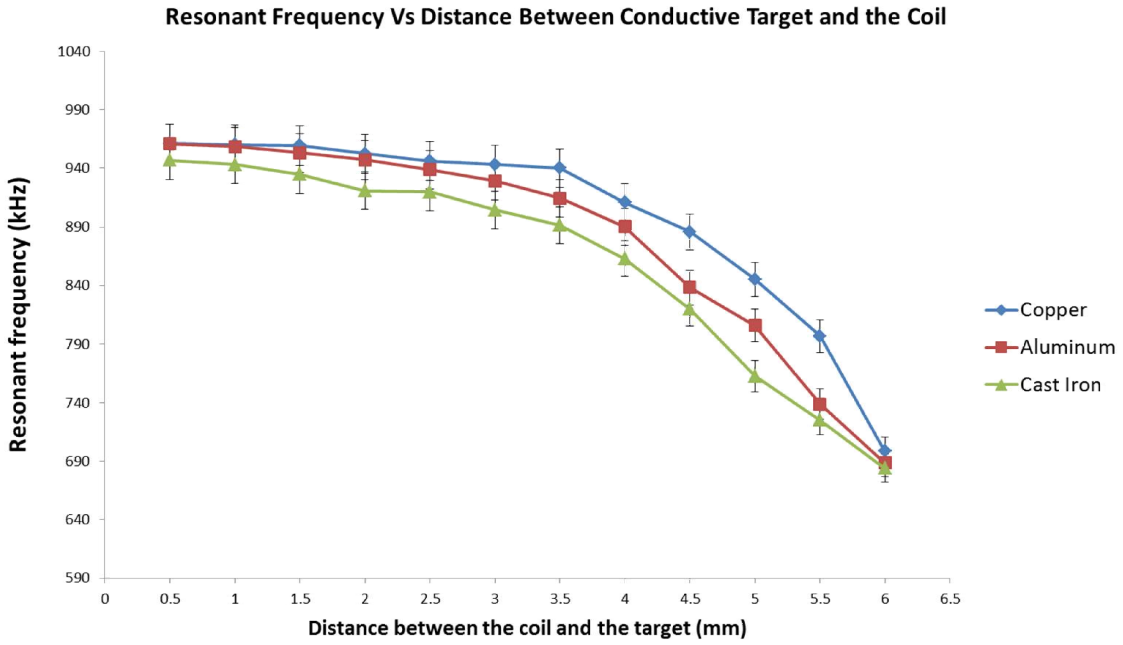

Figure 4.2: Resonant frequency versus distance between different conductive target materials and the fabricated square shaped PCB coils averaged over the four samples in the array. The error bars show the standard error based on 10 samples for each data point.

When testing the fabricated square PCB sensor coils using the conductive composite polymer as the conductive target to determine the effect on the resonant frequency, it was evident that the generated field by the coil did not have measurable effect on the conductive material. We did not observe any changes in the oscillation frequency of the coil. We will provide an explanation for this behavior in section 4.2.2. However, by pressing on the fascia and bringing the conductive composite target in contact with the coil, a significant change was seen in the inductance of the coil. It was observed that the average measured resonance frequency of the four coils in the array was increased by 40% ± 5% when the interface was pressed down by the user for both geometries. The percentage changes in the measured values were significant enough to exceed the threshold values and therefore were detected as a user's touch.

4.2. Experimental Procedures and Results for Binary Switch Sensor

In this section the fabricated coils were examined and characterized. The effect of eddy currents on the binary switch sensor system is discussed. Internal resistance of the coils and inductance changes when flexed at different angles are characterized. The experiments are meant to represent bending occurring during normal use of a flexible device and show that the sensor remains functional during such movements.

4.2.1. Characterization of Binary Switch Sensor Devices Using Conductive Composite Polymer

Both circular and square geometry coils were fabricated with conductive composite polymer with 7 turns, and a line trace thicknesses of approximately 300μm and line spacing of 500 μm to allow ease of demolding of the structures. As mentioned earlier in Chapter 2, the smaller the number of turns in the design, the smaller the inductance of the coil. Because of the lower number of turns in the polymeric coils imposed by limitations in fabrication technique, line width and spacing ratio were chosen such that the inductance of each coil was maximized for the occupied area. The diameter of the circular coil and the longest side length of the square coil were both 20mm. Figure 4.3 shows fabricated circular and square polymeric coils (left) with fabricated interface on top of them (right).

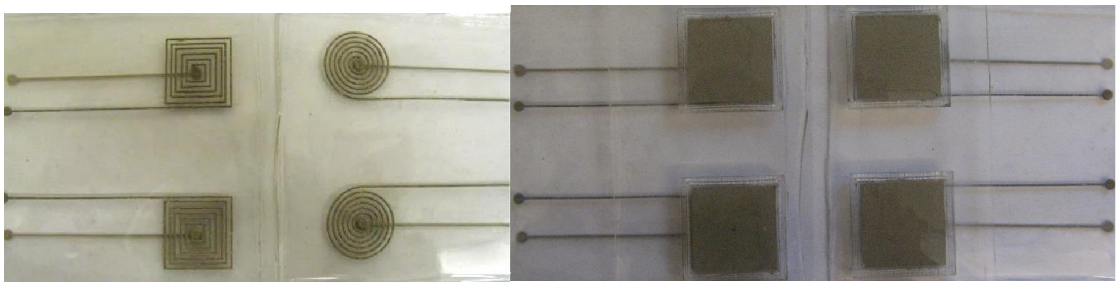

Figure 4.3. Fabricated circular and square flexible coils using composite polymer (left). Placement of the interface on top of the coils (right). The two elements (interface and the coils) were bonded together using silicone sealant to make a single structure before the testing was done.

Similar to the coils made of flexible PCB, identically designed polymeric coils also show variation in their measured inductance. Equation 22 in Chapter 2 furthermore suggests that, given two otherwise identical coils, the one with square spiral geometry should have a higher inductance value compared to the one with circular geometry. The obtained results agree with what Equation 22 suggests: Although the measured inductance values are shifted because of the internal resistance of the coil caused by antiresonance, the averaged inductance values of the square coils in the array are 6.5% higher compared to what was obtained from the circular coils.

The variance in the measured values of identical structures can be attributed to the slight differences in the internal resistance of the coils, the error in the measured frequency by the detection circuit and slight variation in line width and line thickness of the coils. Given the limited resolution of the laser cutter, and also the fact that the laser cutter beam has to be focused manually, variation in characteristics of the coils' trace lines is expected. However, this does not pose a problem in the system, as the change in the inductance and not the initial inductance itself identifies as the user's touch. Variations between devices can be easily removed through software calibration.

4.2.2. Change in Resonance Frequency When Activating the Switch

When testing the conductive composite polymer as the conductive target to determine the presence of eddy currents, it was evident that the generated field by the coil did not have measurable effect on the conductive material. We did not observe any changes in the oscillation frequency of the coil. This can be explained by the relatively lower conductivity of the material compared to copper or aluminum. The electromagnetic forces that move the electrons in the conductive target to create the eddy currents are weak. These forces act on the electrons of the conductive polymer; however, the resistivity of the material actively damps the electron movements, stopping the formation of the eddy current. As a result we could not observe any detectable change in the measured resonant frequency of the material when the conductive polymer was in the range of the sensing coil. However, by pressing on the fascia and bringing the conductive composite target in contact with the coil, a significant change was seen in the

inductance of the coil. It was observed that the average measured resonance frequency of the four coils in the array was increased by 35% ± 5% when the interface was pressed down by the user for both geometries. The percentage changes in the measured values were significant enough to exceed the threshold values and therefore were detected as a user's touch.

4.2.3. Inductance Measurement Vs Angle

The impact of mechanical bending on the sensor behavior and the change in the coils' inductance values were next characterized in order to determine if bending the structure would pose a problem in the detection mechanism of the touch sensor. In this section, the inductance of both square and circular coil geometries over four samples was examined by measuring their resonant frequencies while bending the structure at different angles. Each sample was bent at the center of the coil as shown in the Figure 4.4. The flexing angle was increased in steps of 10° from -40° to 40° (in both inward and outward directions) and the corresponding frequency values were recorded at each angle. Figure 4.4 represents measured frequency at different angles for circular and square coils averaged over the four identical samples.

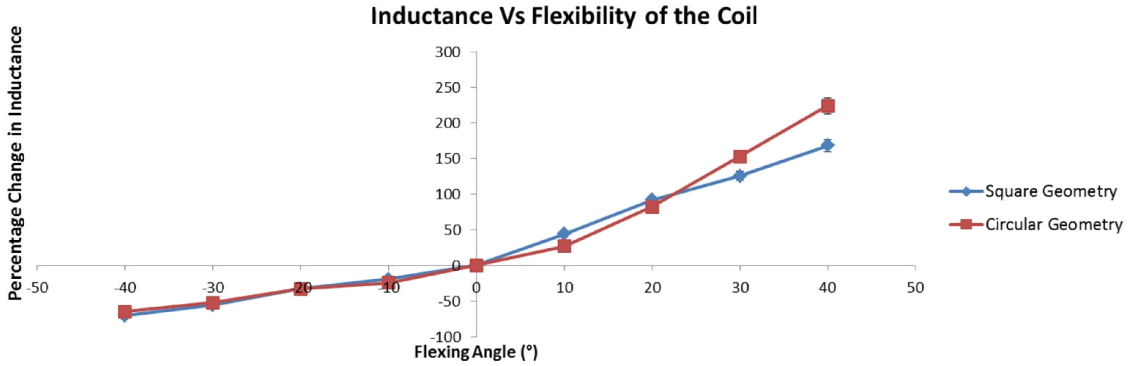

Figure 4.4: Inductance Vs flexibility of the coil. The inductance value tends to increase when the coils are bent inward and conversely decrease when bent outward.

By looking at the Figure 4.4 an interesting trend emerges. The inductance value tends to increase when the coils are bent inward and conversely decrease when bent outward. According to Equation 21, the inductance of a coil is directly proportional to the distance between the coil lines through the outer diameter and the fill ratio. By bending

the coils sensors, the relative distance between the lines also change slightly and cause a shift in the measured values. For example when bent inward, since the coils takes a concave shape, the distance between the coil lines decreases compared to when the coil was flat and therefore an increase in the inductance value was observed. In addition, piezoresistive properties of the coil may play a role in the shift in measured frequency, although prior work has shown that this effect may not be as important, at least in the case of Ag nanoparticle/PDMS composite materials [56]. When flexed, the resistance of the coil may change, which in turn, because of antiresonance phenomenon previously explained, causes the measured frequency to also change.

4.2.4. Internal Resistance of the Coils

As shown in Figure 4.7 for a 15 mm by 50 mm structure, both the internal resistance of the conductive polymer and the change in the resistance when the structure is flexed are in the range of a few tens of ohms. This internal resistance varies depending on the length of the wire that creates the coil: the longer the wire is the higher the number of turns in the coil and the higher internal resistance. The average resistance value of the square and circular coils measured over four samples was measured to be 162 Ω and 140 Ω, respectively, when flat. The resistance of the circular coil is lower than that of the square coil because, geometrically, the circular shape results in a shorter wire length. The relatively high resistance of the fabricated polymeric coils compared to the structures made from flexible PCB can be explained by the lower conductivity of the CCP. Zoflex® CCP has a conductivity 117,400 times lower than that of copper (see Table 3). In addition, random distribution and the shape of the conductive composite particles in the polymer may result in imperfections in the polymer lattice, consequently reducing the conductivity of the coil trace lines [57]. Coils with such a high resistivity result in a very low inductance, and therefore cannot be used as part of eddy current sensor system. When used to measure the frequency of oscillation due to eddy current generation, the change in the inductance is so minimal, that it cannot be distinguished by the detection circuit. As a result, the fabricated polymeric coils are not suitable for creating eddy current sensors, although they work fine as binary touch sensors.

4.3. Characterization of the CCP

In this section, the electrical properties of the conductive composite polymer are discussed. Test structures were fabricated to test the resistivity of CCP when flexed.

4.3.1. Resistivity versus Angle of Deflection

There are different methods to measure the resistivity of a sample. A two-wire measurement is the simplest method for resistance measurement and is used for general assessment of conductivity of a device or component. It is widely used in conventional multimeters, and the readings include the contact resistance of the probes and the series leads' resistances that introduce an error in the range of several milliohms. In most cases these errors are negligible compared to the actual resistances being measured and do not exceed the acceptable error range. This method is best used for resistances between 10Ω to 10 MΩ. Another method is the three-wire measurement (also known as fall of potential method) which is used for measuring high resistance values, typically above 10 MΩ, and can determine insulation resistance. This method uses a third lead as a guard and therefore eliminates the resistance in parallel with the device under test, given that the other two current carrying leads are of the same resistance. The measurement is done by applying a voltage and measuring the resulting short-circuit current [58].

Four-point probe resistance measurement is highly accurate when measuring resistances below 10Ω and is commonly used in low resistance ohmmeters. This method eliminates errors caused by load and contact resistance in the final readings, ensuring a more accurate measurement. Four-point probe measurement passes a current into the sample through two leads (input) and measures the magnitude of the current. The potential across the sample is measured at the same time though another two leads (sensing probes) and the resistance is calculated using the Ohm's law. Since the sensing probes have high impedance, the current cannot flow into the sensing loop and therefore the probes' resistance does not influence the readings. Furthermore, since no current flows through the sensing probes, the contact resistance produced by these

probes does not change the measured potential. Figure 4.5 shows the basic operation of the four-point probe resistance measurement.

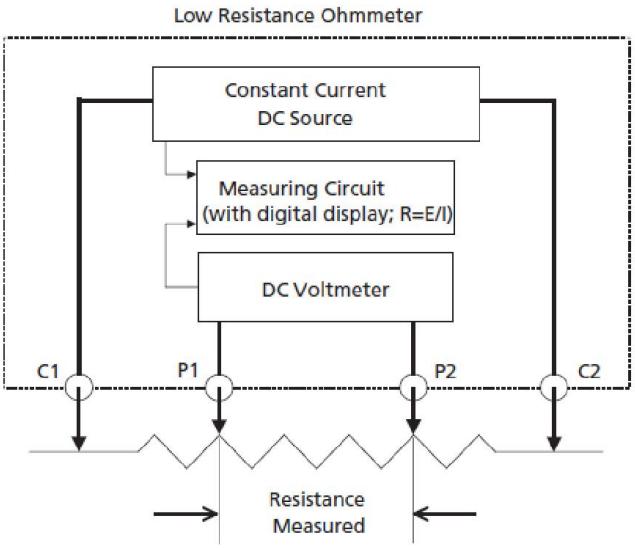

Figure 4.5: Basic operation of four-point probe resistance measurement [59].

For the electrical characterization of the conductive composite polymer, the four-point probe method was chosen since the expected change in the resistivity of the samples caused by change in the thickness of the composite layer or flexing the sample should be so small that regular ohmmeters (two-point probe) would not be expected to measure the difference.

In order to characterize the Zoflex ® composite polymer, three sample films of size 15 mm by 50 mm with thicknesses of 50, 100 and 150 μm were made on a PMDS membrane. Using an HP-3478A multimeter with its leads connections as shown in Figure 4.6, the resistance of each sample was measured. The same experiment was then repeated while flexing the sample at different angles to study the change in the resistance. The flexing angle was increased from a relaxed position in steps of 10° to a maximum of 90° and the corresponding resistance values were recorded at each angle.

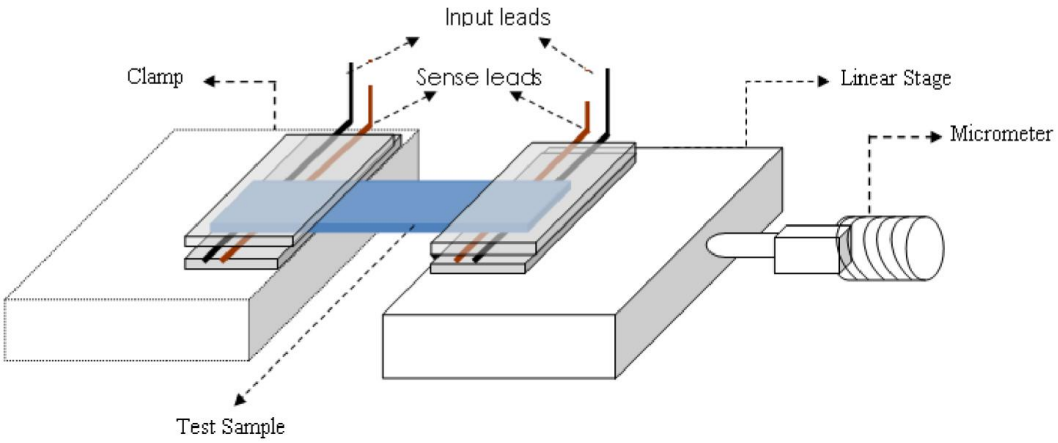

Figure 4.6: Experimental setup to measure the resistivity of CCP samples using HP-3478A multimeter by four-point probe testing [50].

A clear trend was observed from the values and shown in Figure 4.7. As depicted in the figure, the resistance tends to lower as the thickness of the conductive polymer increases. For all three of the samples, it can be seen that the resistance is directly proportional to the flexing angle. This can be explained by random distribution and the shape of conductive composite particle in the polymer lattice. Consequently when flexed, the particles in the lattice rearrange and therefore result in change in resistivity.

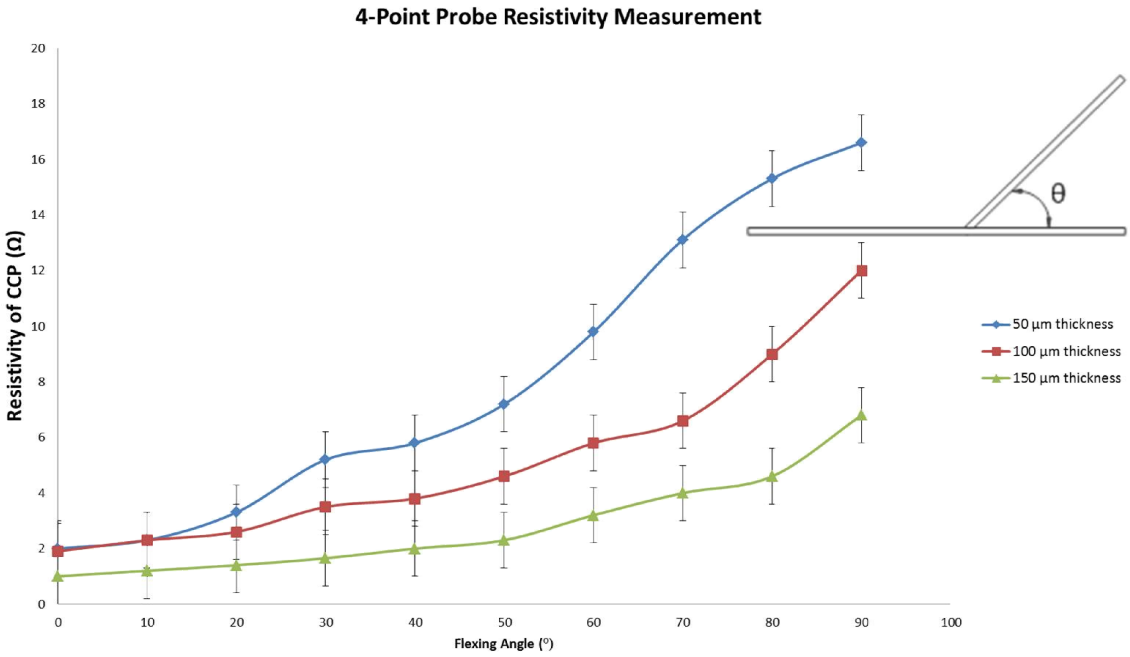

Figure 4.7: **Graph of resistivity of CCP Vs flexing angle using 4-point probe measurement for samples of 15 mm by 50 mm with a thicknesses of 50, 100 and 150µm. A sample with a higher thickness has a lower resistance, and the measured resistance is directly proportional to the flexing angle.**

Chapter 5.

Future Work, Contributions and Concussion

5.1. Future work

In the course of the work discussed in this thesis, several areas were identified for improvement and/or optimization.

Fabrication of the micro-coils on the PCB can be further miniaturized which should result in sensors with smaller footprint. Using a technique described in [60] a minimum feature size of 5μm can be accomplished. Furthermore, the number of turns in the sensor coil can be reduced by placing a known inductor in series with the coil as explained in section 2.4.1 (Figure 2.10). Although a smaller number of turns results in a smaller inductance, because of the accuracy of the detection circuit used, preliminary results show the changes in the inductance caused by the user can still be detected.

Further miniaturizing of the sensor elements as well as creating a much denser sensor array can create a system that is capable of detecting proximity of a target, contact and flexion. A positioning algorithm called the *event analyzer* needs to be implemented to obtain a spectrum of the measured inductances in a large array of sensors. This spectrum is a plot of percentage change in the inductance of the sensors and location of the sensors in the 2D plane as shown in Figure 5.1. The spectrum is a function of the distance between the sensing coil and the touch event, as well as between the sensing coil and the target material that is in proximity of the sensor, and shows both the location of the event on the surface of the sensor array and the combined effect of the event on all the sensors.

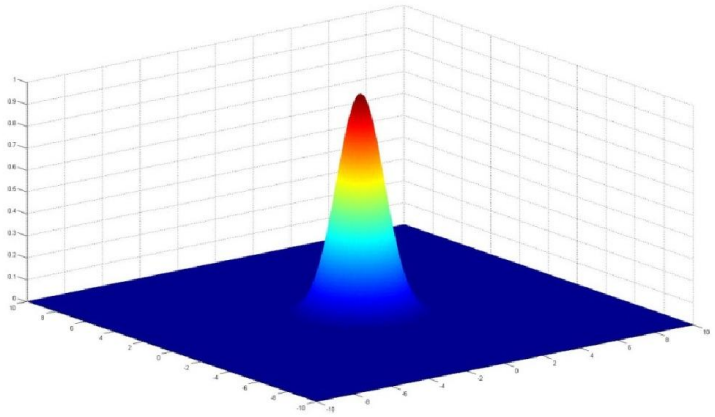

Figure 5.1: Event analyzer spectrum showing maximum inductance change occurred at location (0,0) indicating location of the touch on the sensor array plane.

The event analyzer spectrum should also have a peak at the contact location called the *event-peak*, and a plateau caused by the nearby sensor elements affected by the event. Using event analyzer algorithm, multiple events that occur at the same time can be distinguished given enough distance between their respective event-peaks. For those overlapping events, depending on the application of the sensor array, software interpretation and further analysis is required to determine proper interpretation of the events.

In addition, a firmware algorithm can be changed in order to support velocity sensitivity which can lead to new applications that the sensor can be used in. The faster the user presses, the more sudden the change in the measurement will be. The firmware can be altered to store previous measurement values for a defined period of time and compare them with the current measurement (as oppose to comparing the measurement value with initial values). Then incremental percentage changes can be calculated to determine how fast the touch sensor was pressed.

One of the disadvantages of using the thin cooper film as the target is that it is not stretchable and is prone to metal fatigue when stretched. The Microinstrumentation Laboratory at SFU has developed a new low cost thick-film metallization transfer process onto PDMS that utilizes a sacrificial conductive cooper paint [61]. This method

embeds the microstructures flush with the PDMS surface and produces a metallization layer that adheres to PDMS without the need for surface modification. A dry film photoresist layer is laminated on top and patterned using standard techniques. Next, the electroplated cooper is grown on the seed layer through the photoresist mask and transferred to PDMS through a unique baking procedure. Structures fabricated using this new process have shown reliability under flexing during initial experiments. New methods to increase the flexibility of the copper microstructures are also being investigated. When this method is fully developed, it may be adopted and integrated with this work to alleviate the problems that can arise from using thin copper film. However, the resolution of this method is currently limited to 100 micrometers with a film thickness of 25-75 micrometers. Another point related to the sensor's target that that can be investigated would be the shape of the target. Currently a square shaped target is the only shape used in this project due to its simplicity. Other target geometries can be investigated to test their effect on sensitivity and response of the system as well as their effect on the eddy current generation. In addition, a target in the form of a secondary coil that mirrors the sensor coil is another area to investigate [17].

In addition, a different method for the preparation and micromolding of flexible electrically conducting nanocomposite polymers has been investigated in the Microinstrumentation Laboratory. For example, Khosla et.al in [62] demonstrated preparation of a different polymer using ultrasonic agitation with multi-walled carbon nanotubes (MWCNT) in polydimethylsiloxane (PDMS). In addition, electrically conducting Silver nanoparticle (Ag-n) doped PDMS nanocomposite has also been used in fabricating and micropatterning flexible structures. Demonstrated in [50], silver nanoparticles (with an average diameter of 80 nm and 99.5% purity) uniformly dispersed in the PDMS nanocomposite form a highly flexible conductive circuits. Combining those nanocomposite polymers and the preparation methods presented in these papers with the Zoflex® conductive composite polymer will be investigated to create a highly flexible nanocomposite polymer that has a conductivity that is 10 to 100 times compared to Zoflex® [50], [63]. This would increase the inductance of the polymeric coils and stronger magnetic field and thus allow their use as a proximity sensor in addition to a binary switch.

Finally, additional testing could enable the sensor to be employed for a wider variety of applications than a touch sensor. For example, pressure versus deflection would give insight into using the eddy-current sensor for more complex tactile information. Furthermore, the response speed of the sensor qualitatively was fast enough (estimated at less 0.5 ms) but was not specifically characterized. While the response was qualitatively fast enough for the intended use as a switch, further characterization would determine the usability of the sensors for more complex tactile measurements, e.g., for manipulation of objects.

5.2. Contributions

This thesis aims has made the following contributions to the field of flexible touchpads based on inductive sensing principles:

1. Development of two tactile sensor array technologies (eddy-current and binary-switch based) that use inductance as a transduction principle that can be implemented in flexible wearable systems.

2. Development of a general fabrication process for inductive tactile sensors using flexible printed circuit board (PCB) technology, as well as micromolding processes of conductive composite polymers on flexible polymer membranes.

3. Development of a modeling framework for design of inductive sensor coils using finite element analysis tools to study the characteristics of their generated magnetic field.

4. Development of a detection system in the form of both software and hardware that interfaces with a flexible inductive sensor array that can detect and respond to user stimulus.

Partial results of the work reported in this thesis was presented at the *2014 SPIE Smart Structures and Material Systems + Nondestructive Evaluation and Health Monitoring Annual International Symposium* in San Diego, California and was published in its proceeding under “Flexible touchpads based on inductive sensors using embedded conductive composite polymer” in 2014 [28]. Some of the fabrication techniques used in this thesis were also used in a side project which is published in the proceeding of *SPIE Nanosystems in Engineering and Medicine* under “Manipulation of permanent magnetic

polymer micro-robots: a new approach towards guided wireless capsule endoscopy" in 2012 [64].

5.3. Summary and Conclusion

The aim of the work carried out in this thesis was to develop a polymer based flexible array of sensor switches intended for applications in wearable electronics and sensor systems. Two designs were demonstrated to achieve a flexible tactile sensor that work based on inductive principles because of their performance capabilities, simplicity in design, not being bulky, requiring simple signal processing, temperature independence and repeatability, and showing long term stability.

In the first design, a tactile sensor that works based on the principle of eddy current was demonstrated. This method can also be used as a proximity sensor where the sensing element can detect the proximity of any conductive material. The second design uses the contact between the conductive target and the sensing coil to detect a touch. This approach results in a binary switch that can detect two states of contact and non-contact. Unlike currently existing inductive sensors that are usually bulky in size, both systems are based on thin polymeric materials and feature a simple design that gives them an advantage over existing solutions.

To achieve the goals of this thesis work, a scientific understanding of the transduction principles were established. A preliminary investigation of the sensor system design based on resonant circuit theory was presented. Detailed analysis of the sensor coil behavior was conducted by performing a Finite Element Analysis using COMSOL. Based on these analyses, the final design took into consideration the device size and the tradeoff between coil geometry and the resulting coil inductance.

Through the use of MEMS technology and micro molding processes, flexible polymer based coils were developed to act as the devices' sensing elements. Such an approach has several advantages, such as batch fabrication; low cost manufacturing; potential to further miniaturization to create high density sensor arrays; and integration of the sensor device with other MEMS, polymer based, wearable or flexible systems. In

comparison with other reported MEMS inductive tactile sensors, the sensors designed in this work exhibit a high degree of flexibility and are significantly less bulky. In addition, the fabrication methods adopted in this work uses fewer fabrication process steps.

The detection mechanism demonstrated in this work is a simple detection circuit compared to other existing touch sensor systems (such as capacitive sensors that are susceptible to cross talk and noise and thus require analog compensation). The simplicity of the detection circuit does not hinder its accuracy and we were able to accurately measure known inductors as low as 500 nH. During the design of the detection circuit, expandability of the system was taken into account to facilitate realization of a single chip supporting an array of sensors. Any calibration, varying sensitivity, or signal processing can be achieved by changes to the software: changing threshold values or the touch event detection algorithm, for example.

Finally, the resulted tactile sensor prototypes that have been developed in this work consisted of an array of 4 sensors. The sensors developed were characterized to study their physical characteristics and performance under different circumstances. The impact of mechanical bending on the sensor behavior and the change in the coils' inductance values were characterized in order to determine if bending of the structure poses a problem in the detection mechanism of the touch sensor. In addition, sensor coils were examined to study the effect of generated eddy currents on the resonant frequency by changing the distance between the coil and the target. As shown in chapter 4, the frequency output of the coil exhibits non-linear characteristics when the target distance changes. Rather than focusing on developing a device with linear output characteristics, the work was geared toward development and optimization of the software with performance capability analogous to ones defined in the thesis objectives. Again, this shows how easily sensitivity and detection range of the device can be manipulated through signal processing. The sensitivity of both types of sensors, along with each sensor's detection mechanism, were found to be sufficient to allow detection of user's touch.

References

[1] H. R. Nicholls and M. H. Lee, “A Survey of Robot Tactile Sensing Technology,” *The International Journal of Robotics Research*, vol. 8, no. 3, pp. 3–30, Jun. 1989.

[2] H. B. Muhammad, “Development of a bio-inspired MEMS based tactile sensor array for an artificial finger,” d_ph, University of Birmingham, 2012.

[3] J. Dargahi and S. Najarian, “Human tactile perception as a standard for artificial tactile sensing--a review,” *Int J Med Robot*, vol. 1, no. 1, pp. 23–35, Jun. 2004.

[4] R. Agrawal, R. C. Jain, R. K. Jaina, and U. of M. C. of E. C. for R. on I. M. R. S. Division, *An Overview of Tactile Sensing*. Robot Systems Division, College of Engineering, the University of Michigan, 1986.

[5] A. Wisitsoraat, V. Patthanasetakul, T. Lomas, and A. Tuantranont, “Low cost thin film based piezoresistive MEMS tactile sensor,” *Sensors and Actuators A: Physical*, vol. 139, no. 1–2, pp. 17–22, Sep. 2007.

[6] M. I. Tiwana, S. J. Redmond, and N. H. Lovell, “A review of tactile sensing technologies with applications in biomedical engineering,” *Sensors and Actuators A: Physical*, vol. 179, pp. 17–31, Jun. 2012.

[7] H. Yousef, M. Boukallel, and K. Althoefer, “Tactile sensing for dexterous in-hand manipulation in robotics—A review,” *Sensors and Actuators A: Physical*, vol. 167, no. 2, pp. 171–187, Jun. 2011.

[8] C. Steinem and A. Janshoff, Eds., *Piezoelectric sensors*. Berlin ; New York: Springer, 2006.

[9] P. Puangmali, K. Althoefer, L. D. Seneviratne, D. Murphy, and P. Dasgupta, “State-of-the-Art in Force and Tactile Sensing for Minimally Invasive Surgery,” *IEEE Sensors Journal*, vol. 8, no. 4, pp. 371–381, 2008.

[10] S. B. Lang and S. Muensit, “Review of some lesser-known applications of piezoelectric and pyroelectric polymers,” *Appl. Phys. A*, vol. 85, no. 2, pp. 125–134, Nov. 2006.

[11] P. Ueberschlag, “PVDF piezoelectric polymer,” *Sensor Review*, vol. 21, no. 2, pp. 118–126, Jun. 2001.

[12] P. Dario, M. Bergamasco, A. Fiorillo, and R. Leonardo, “Geometrical optimization criteria for the design of tactile sensing patterns,” in *1986 IEEE International Conference on Robotics and Automation. Proceedings*, 1986, vol. 3, pp. 1268–1273.

[13] V. Maheshwari and R. Saraf, “Tactile Devices To Sense Touch on a Par with a Human Finger,” *Angewandte Chemie International Edition*, vol. 47, no. 41, pp. 7808–7826, 2008.

[14] D. De Rossi, G. Canepa, G. Magenes, F. Germagnoli, A. Caiti, and T. Parisini, “Skin-like tactile sensor arrays for contact stress field extraction,” *Materials Science and Engineering: C*, vol. 1, no. 1, pp. 23–36, May 1993.

[15] Y. Hasegawa, H. Sasaki, M. Shikida, K. Sato, and K. Itoigawa, “Magnetic actuation of a micro-diaphragm structure for an active tactile sensor,” in *Proceedings of the 2004 International Symposium on Micro-Nanomechatronics and Human Science, 2004 and The Fourth Symposium Micro-Nanomechatronics for Information-Based Society, 2004*, 2004, pp. 99–104.

[16] S. Takenawa, “A magnetic type tactile sensor using a two-dimensional array of inductors,” in *IEEE International Conference on Robotics and Automation, 2009. ICRA ’09*, 2009, pp. 3295–3300.

[17] C. Lucarotti, C. M. Oddo, N. Vitiello, and M. C. Carrozza, “Synthetic and Bio-Artificial Tactile Sensing: A Review,” *Sensors*, vol. 13, no. 2, pp. 1435–1466, Jan. 2013.

[18] S. Tumanski, “Induction coil sensors—a review,” *Meas. Sci. Technol.*, vol. 18, no. 3, p. R31, Mar. 2007.

[19] M. A. Brown and R. C. Semelka, *MRI: Basic Principles and Applications*. John Wiley & Sons, 2011.

[20] M. R. Nabavi and S. N. Nihtianov, “Design Strategies for Eddy-Current Displacement Sensor Systems: Review and Recommendations,” *IEEE Sensors Journal*, vol. 12, no. 12, pp. 3346–3355, Dec. 2012.

[21] H. X. A, J. S. Z. A, and H. C. B, *Laparoscopic surgery, perceptual limitations and force: A review*. .

[22] A. M. Okamura, “Haptic Feedback in Robot-Assisted Minimally Invasive Surgery,” *Curr Opin Urol*, vol. 19, no. 1, pp. 102–107, Jan. 2009.

[23] M. E. H. Eltaib and J. R. Hewit, “Tactile sensing technology for minimal access surgery—a review,” *Mechatronics*, vol. 13, no. 10, pp. 1163–1177, Dec. 2003.

[24] T. Liu, Y. Inoue, and K. Shibata, “A Small and Low-Cost 3-D Tactile Sensor for a Wearable Force Plate,” *IEEE Sensors Journal*, vol. 9, no. 9, pp. 1103–1110, Sep. 2009.

[25] R. K. Kramer, C. Majidi, and R. J. Wood, “Wearable tactile keypad with stretchable artificial skin,” in *2011 IEEE International Conference on Robotics and Automation (ICRA)*, 2011, pp. 1103–1107.

[26] Y. Hasegawa, M. Shikida, D. Ogura, Y. Suzuki, and K. Sato, “Fabrication of a wearable fabric tactile sensor produced by artificial hollow fiber,” *J. Micromech. Microeng.*, vol. 18, no. 8, p. 085014, Aug. 2008.

[27] M. I. Tiwana, “Design of tactile sensors for robotic hand control and upper limb prostheses,” Ph.D., Faculty of Engineering, UNSW, 2012.

[28] A. Rahbar, M. Rahbar, and B. L. Gray, “Flexible touchpads based on inductive sensors using embedded conductive composite polymer,” 2014, p. 90600O.

[29] C. Reig, S. Cardoso, and S. Mukhopadhyay, *Giant Magnetoresistance (GMR) Sensors: From Basis to State-of-the-Art Applications*. Springer Science & Business Media, 2013.

[30] P. Reghem, E. Destobbeleer, T. Derrey, and L. Protin, “Precision of an eddy current sensor with magnetic circuit losses,” in *, 20th International Conference on Industrial Electronics, Control and Instrumentation, 1994. IECON ’94*, 1994, vol. 2, pp. 915–919 vol.2.

[31] M. Rahbar, S. Seyfollahi, A. Khosla, B. L. Gray, and L. Shannon, “Fabrication Process for Electromagnetic Actuators Compatible with Polymer Based Microfluidic Devices,” *ECS Trans.*, vol. 41, no. 20, pp. 7–17, May 2012.

[32] D. D. Hilbich, A. Khosla, B. L. Gray, and L. Shannon, “Bidirectional magnetic microactuators for uTAS,” 2011, vol. 7929, p. 79290H–79290H–11.

[33] A. Khosla and B. L. Gray, “Magnetic Elastomeric Polymers for Soft MEMS: Fabrication and Process Technology,” *Meet. Abstr.*, vol. MA2010–02, no. 42, pp. 2338–2338, Jul. 2010.

[34] A. Khosla, J. Herchenroeder, D. Miller, and Z. Chen, “Polymeric Permanent Magnetic Micro-Actuators,” *Meet. Abstr.*, vol. MA2011–01, no. 45, pp. 2057–2057, Mar. 2011.

[35] K. Hashimoto, *RF Bulk Acoustic Wave Filters for Communications*. Artech House, 2009.

[36] S. A. Dyer, *Wiley Survey of Instrumentation and Measurement*, 1 edition. New York: Wiley-IEEE Press, 2001.

[37] Y. Yating, D. pingan, and W. Zhenwei, “Study on the electromagnetic properties of eddy current sensor,” in *Mechatronics and Automation, 2005 IEEE International Conference*, 2005, vol. 4, pp. 1970–1975 Vol. 4.

[38] D. J. Sadler and C. H. Ahn, “On-chip eddy current sensor for proximity sensing and crack detection,” *Sensors and Actuators A: Physical*, vol. 91, no. 3, pp. 340–345, Jul. 2001.

[39] K. L. Kaiser, *Electromagnetic Compatibility Handbook*, 1 edition. Boca Raton: CRC Press, 2004.

[40] P. A. Tipler and G. Mosca, *Physics for Scientists and Engineers, Volume 2: Electricity, Magnetism, Light, and Elementary Modern Physics*. Macmillan, 2004.

[41] T. H. Glisson, *Introduction to Circuit Analysis and Design*, 2011 edition. S.l.: Springer, 2011.

[42] P. E. M., P. E. E.E, *Introduction to Nondestructive Testing: A Training Guide*. John Wiley & Sons, 2005.

[43] H. A. Wheeler, “Simple Inductance Formulas for Radio Coils,” *Proceedings of the Institute of Radio Engineers*, vol. 16, no. 10, pp. 1398–1400, Oct. 1928.

[44] S. S. Mohan, M. del Mar Hershenson, S. P. Boyd, and T. H. Lee, “Simple accurate expressions for planar spiral inductances,” *IEEE Journal of Solid-State Circuits*, vol. 34, no. 10, pp. 1419–1424, Oct. 1999.

[45] “Electromagnetics Software - Computational Electromagnetics Modeling.” [Online]. Available: http://www.comsol.com/acdc-module. [Accessed: 06-Aug-2014].

[46] “Very Accurate LC Meter based on PIC16F628A,” *electronics-DIY*, 05-Feb-2014. [Online]. Available: http://electronics-diy.com/lc_meter.php. [Accessed: 05-Feb-2014].

[47] P. Stoffregen, *FreqCount Library*. PJRC.COM, LLC, 2014.

[48] J. Liu, B. Cai, J. Zhu, G. Ding, X. Zhao, C. Yang, and D. Chen, “Process research of high aspect ratio microstructure using SU-8 resist,” *Microsystem Technologies*, vol. 10, no. 4, pp. 265–268, May 2004.

[49] M. Rahbar, “PMMA microfluidics technology: development and characterization,” Thesis, Applied Science: School of Engineering Science, 2010.

[50] A. Khosla, “Micropatternable multifunctional nanocomposite polymers for flexible soft MEMS applications,” Thesis, Applied Science: School of Engineering Science, 2011.

[51] S. K. Chhina, “Microfluidic system to detect select DNA fragments using agglutination process,” Thesis, Applied Science: School of Engineering Science, 2011.

[52] K. Haubert, T. Drier, and D. Beebe, “PDMS bonding by means of a portable, low-cost corona system,” *Lab Chip*, vol. 6, no. 12, pp. 1548–1549, Nov. 2006.

[53] W. D. Callister and D. G. Rethwisch, *Materials Science and Engineering: An Introduction*, 8 edition. Hoboken, NJ: Wiley, 2009.

[54] A. Shadowitz, *The Electromagnetic Field*. New York: Dover Publications, 2010.

[55] J. D. Kraus and J. D. Kraus, *Electromagnetics*, 4 edition. New York: Mcgraw-Hill College Division.

[56] D. Chung, “Flexible conductive polymer electrodes for applications in tissue Electrical Impedance Scanning (EIS),” Thesis, Applied Science: School of Engineering Science, 2012.

[57] Y. P. Mamunya, V. V. Davydenko, P. Pissis, and E. V. Lebedev, “Electrical and thermal conductivity of polymers filled with metal powders,” *European Polymer Journal*, vol. 38, no. 9, pp. 1887–1897, Sep. 2002.

[58] “Multi-Terminal Impedance Measurement.” Chroma, May-2014.

[59] “A Guide to Low Resistance Testing: Understanding and Measuring Low Resistance to Ensure Electrical System Performance.” Megger, 01-Jan-2014.

[60] E. T. Enikov and K. Lazarov, “PCB-integrated metallic thermal micro-actuators,” *Sensors and Actuators A: Physical*, vol. 105, no. 1, pp. 76–82, Jun. 2003.

[61] D. Hilbich, A. Khosla, L. Shannon, and B. L. Gray, “A new low-cost, thick-film metallization transfer process onto PDMS using a sacrificial copper seed,” 2014, p. 906007.

[62] A. Khosla and B. L. Gray, “Preparation, characterization and micromolding of multi-walled carbon nanotube polydimethylsiloxane conducting nanocomposite polymer,” *Materials Letters*, vol. 63, no. 13–14, pp. 1203–1206, May 2009.

[63] X. Z. Niu, S. L. Peng, L. Y. Liu, W. J. Wen, and P. Sheng, “Characterizing and Patterning of PDMS-Based Conducting Composites,” *Adv. Mater.*, vol. 19, no. 18, pp. 2682–2686, 2007.

[64] D. Hilbich, A. Rahbar, A. Khosla, and B. L. Gray, “Manipulation of permanent magnetic polymer micro-robots: a new approach towards guided wireless capsule endoscopy,” 2012, p. 85482I.